

Received by OSTI

MAY 20 1992

DOE/ER/40592-2

Nuclear Physics at Extreme Energy Density

Progress Report

May 1991 - April 1992

BERNDT MÜLLER

Department of Physics

Duke University

Durham, NC 27706

15 May 1992

DISCLAIMER

This report was prepared as an account of work sponsored by an agency of the United States Government. Neither the United States Government nor any agency thereof, nor any of their employees, makes any warranty, express or implied, or assumes any legal liability or responsibility for the accuracy, completeness, or usefulness of any information, apparatus, product, or process disclosed, or represents that its use would not infringe privately owned rights. Reference herein to any specific commercial product, process, or service by trade name, trademark, manufacturer, or otherwise does not necessarily constitute or imply its endorsement, recommendation, or favoring by the United States Government or any agency thereof. The views and opinions of authors expressed herein do not necessarily state or reflect those of the United States Government or any agency thereof.

PREPARED FOR THE U.S. DEPARTMENT OF ENERGY

UNDER GRANT NUMBER DE-FG-5-90ER40592

dlz
DISTRIBUTION OF THIS DOCUMENT IS UNLIMITED

TABLE OF CONTENTS

0.	INTRODUCTION	1
1.	QCD TRANSPORT THEORY	2
1.1.	Relativistic Parton Cascade	2
1.2.	QCD Phenomenology of Nucleon-Nucleon Cross Sections	3
1.3.	Probing Parton Thermalization Time with Charm Production	7
1.4.	Color Screening in Relativistic Heavy Ion Collisions	11
2.	MINIJETS IN HADRONIC AND NUCLEAR COLLISIONS	14
2.1.	Minijets or QGP in $p\bar{p}$ High Energy Collisions?	14
2.2.	Resolving Minijets in Hadronic Interactions	16
2.3.	Gluon Shadowing and Jet Quenching in High Energy $A + A$ Collisions	18
2.4.	Minijet Contribution to the Background of Direct Photons	21
3.	LATTICE GAUGE THEORY	25
3.1.	Deterministic Chaos in Non-Abelian Lattice Gauge Theory	25
3.2.	Thermalization in SU(2) gauge theory	29
4.	HADRONIC MATTER AND OTHER STUDIES	32
4.1.	Nuclear Medium Effect on Kaon Dispersion Relation	32
4.2.	Non-equilibrium Statistical Field Theory	33
4.3.	Applying Neural Networks to Resonance Search	34
4.4.	The formation of $\pi^- \pi^+$ -atoms in relativistic heavy ion collisions	35
4.5.	Finite Volume Effects on Gluon Plasma	36
5.	STRONG ELECTROMAGNETIC FIELDS	39
5.1.	Exact Dirac Propagator in a Magnetic "Sheet"	39
5.2.	W Boson Condensation in p-p Collisions?	40
5.3.	Quark-Antiquark Condensates in Strong Magnetic Fields	42
5.4.	Collective Excitations of the QED Vacuum ?	45
6.	APPENDICES	49

MASTER

INTRODUCTION

Nuclear Physics in the United States and elsewhere is entering an era of investigations focussing on the quark-gluon substructure of nuclear matter. These studies, to be carried out at CEBAF, the Brookhaven AGS, and RHIC, have the same importance for nuclear physics as studies of atomic and molecular substructure have for chemistry and condensed matter physics. Moreover, the investigation of quark-gluon matter at extremely high energy density, which is the primary goal of RHIC, will most likely allow us to probe the influence of the structure of the vacuum state on the laws of physics, and quite possibly yield a first glimpse of "the physics of the next century".

Many theoretical questions remain to be settled, before the experimental search for new phenomena can be carried out with a good chance of success. E.g. we need to find a promising, reliable set of signatures for the change in the structure of nuclear matter from hadrons to a plasma of deconfined quarks and gluons. We need more detailed predictions of quantum chromodynamics for the structure of hadrons and for the phase diagram of hadronic matter. We also need to better understand the mechanism by which (approximate) local thermodynamic equilibrium is established in nuclear collisions at very high energy.

The work of our group over the past two years has focussed on the last of these questions: We have first approached the thermalization problem from the angle of perturbative QCD. This approach should work better as the collision energy is increased and semi-hard scattering phenomena become more abundant. Indeed, the results presented in the body of this report indicate that there may be a direct route at collider energies from the quark-gluon substructure of the colliding nucleons to a locally thermalized quark-gluon plasma, which can be described all the way within the framework of perturbative QCD.

More recently, we have begun nonperturbative investigations of nonequilibrium phenomena in the framework of semiclassical gauge theory on the lattice. These studies have revealed a universal presence of chaotic dynamics of the non-abelian gauge field, and have allowed us to calculate the characteristic growth time of the entropy contained in the gauge field. Our result, first reported here, supports estimates of a very short gluon thermalization time obtained in the context of perturbative thermal QCD, and may have important quantitative implications for many proposed signatures of the quark-gluon plasma.

Finally, the institution of a N.C. Triangle-wide Nuclear Theory (TNT) Colloquium in the Fall of 1991 has fostered the regular communication and exchange of ideas among the nuclear theorists at the three major universities in the area. A regular stream of first-rate speakers has greatly contributed to the exposure of local theorists, experimentalists, and graduate students to recent developments in nuclear theory.

In the following we present an account of the research results obtained by the members of the DOE-supported nuclear theory group at Duke University during the past year. The interested reader will be able to find more details in the publications and preprints listed in the Appendix.

1. QCD TRANSPORT THEORY

This series of projects deals with the earliest stage of a nuclear collision at very high energy, by applying the knowledge of perturbative QCD to gain an understanding of the dynamic processes that eventually lead to local equilibration of energy and, presumably, to the formation of a quark-gluon plasma in those collisions (Fig. 1 visualizes the space-time evolution of a collision event). Several proposed signatures of a quark-gluon plasma are quite sensitive to the initial temperature at which this state is formed. We hope to obtain quantitative insight into the equilibration mechanism through a study of the temporal evolution of parton distributions in the framework of perturbative QCD.

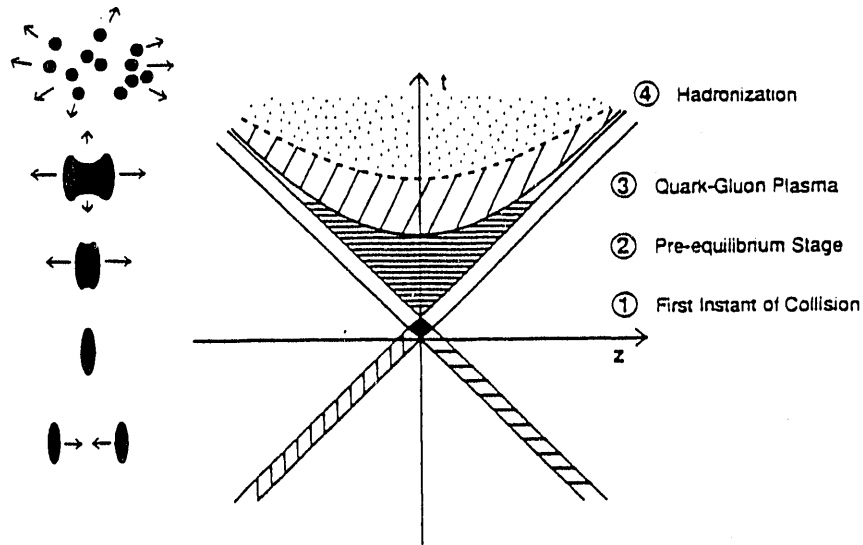


Fig. 1: Space-time picture of a highly relativistic heavy-ion collision.

1.1. Relativistic Parton Cascade

(K. Geiger, B. Müller [*])

Our parton cascade model is a QCD based relativistic kinetic model for high energy nuclear collisions. It is inspired by the parton picture of hadronic interactions and describes the nuclear collision in terms of the space-time evolution of cascades consisting of quarks, antiquarks, gluons and the partons. The nuclear dynamics is traced back to the microscopic level of quark and gluon interactions in the framework of perturbative QCD. This enables us to follow the time development of the nuclear system in space-time by solving a transport equation for the parton distributions by Monte Carlo methods.

We employ a kinetic formulation based on a relativistic covariant transport equation that embodies the following main elements:

1. The nucleons of the colliding nuclei are resolved into their parton substructure according to the measured nucleon structure functions.
2. The evolution of the ensemble of partons during the course of the collision according to the structure of parton interactions as described by perturbative QCD. This includes multiple scatterings together with associated space-like and time-like parton emission processes before, respectively after, each scattering.

We assume factorization of the short range hard and semihard parton-parton scatterings and the hadronization processes mediated by long range confinement forces. In our description we represent the partons as classical point particles of various species as specified by their internal degrees of freedom. The state of a parton is characterized by its flavor $a = q_f, \bar{q}_f, g$, its momentum \vec{p} and position \vec{r} . Its energy is determined by $E^2 = p^2 + m_a^2 + M^2$ where m_a is the rest mass of parton a and M is a possible space-like ($M^2 < 0$) or time-like ($M^2 > 0$) virtual mass ($M^2 = 0$ for partons on mass shell).

As interaction we include the important class of asymptotically dominant ($2 \rightarrow n$) processes which can be obtained from elementary ($2 \rightarrow 2$) interactions followed or preceded by space-like and time-like branchings. For this set of ($2 \rightarrow n$) processes, we formally write the invariant amplitudes squared as

$$\begin{aligned} |\mathcal{M}|_{2 \rightarrow n}^2 &= |(a_1 a_2 \dots b_1 b_2 \dots c_1 c_2 \dots d_1 d_2 \dots cd | \mathcal{M} | ab)|^2 \\ &= [S_a(x_a, Q^2, Q_0^2) S_b(x_b, Q^2, Q_0^2)] |\mathcal{M}_{ab \rightarrow cd}(\hat{s}, \hat{t}, \hat{u}, Q^2)|^2 \\ &\quad \cdot [T_c(Q^2, \mu_0^2) \cdot T_d(Q^2, \mu_0^2)], \end{aligned} \quad (1)$$

where $|\mathcal{M}|_{2 \rightarrow n}$ is the probability that a certain scattering between two partons a and b at $\hat{s}, \hat{t}, \hat{u}$ and Q^2 (the scale of the scattering) will result into n outgoing partons and a_i, b_i are the partons radiated from a, b before the elementary ($2 \rightarrow 2$) scattering $a + b \rightarrow c + d$, and c_i, d_i are the partons radiated from the final state partons c, d . The infrared divergences of the perturbative QCD cross sections were avoided by cut-offs imposed on the invariant momentum transfer p_T^{\min} , and on the parton splitting fraction z_{\min} (see also section 1.2).

Early results obtained with our cascade program were reported in last year's Report, and at the Quark Matter '91 meeting [1]. We found that perturbative QCD processes alone account for a large amount of energy stopping at the RHIC energy range. They also lead to the rapid "thermalization" of transverse momentum, indicated by the presence of an exponential slope in the p_T spectrum of partons after about 1 fm/c [* , 1]. A more rigorous study of the aspects related to energy thermalization by K. Geiger [2], incorporating parton fusion and formation time effects, has shown that the longitudinal as well as transverse motion of partons at central rapidity appears to be equilibrated in collisions at RHIC energy with a slope in the momentum spectrum corresponding to a temperature around 300 MeV.

[*] K. Geiger and B. Müller, Nucl. Phys. B **369**, 600 (1992).

[1] K. Geiger, Dynamics of Parton Cascades in Highly Relativistic Nuclear Collisions, Proc. Quark Matter '91 (to be published in Nuclear Physics A).

[2] K. Geiger, Thermalization in Ultra-Relativistic Nuclear Collisions, Univ. Minnesota preprint, March 1992.

1.2. QCD Phenomenology of Nucleon-Nucleon Cross Sections

(N. Abou-El-Naga, K. Geiger, B. Müller [*])

Since inclusive parton cross sections in perturbative QCD are plagued by infrared divergences, the parton cascade model requires the introduction of two cut-off parameters: a lower cut-off p_T^{\min} for the allowed transverse momentum exchange, and a cut-off μ_0 for

the invariant mass of off-mass shell partons in the radiative cascade following a two-parton collision. The value of the μ_0 is known to be intimately connected with the nonperturbative phenomenon of hadronization in QCD, and its value must be chosen in accordance with a particular hadronization scheme. This is different for the momentum cut-off p_T^{\min} , which can be determined from consideration of the total non-diffractive $p + p$, or $p + \bar{p}$ cross section. Studies similar to ours have been made previously by Sjöstrand and van Zijl [1], Durand and Pi [2], Gaisser and Halzen [3], and by Block et al. [4].

At high energies it is useful to work in the impact parameter representation for the nucleon-nucleon scattering amplitude

$$f(t, s) = \frac{i\sqrt{s}}{4\pi} \int d^2b \left(1 - e^{-\chi(b, s)}\right) J_0(b\sqrt{-t}), \quad (1)$$

where t and s are the Mandelstam variables of the two-nucleon system and $\chi(b, s)$ is the complex eikonal function. The total, elastic, and inelastic cross sections can be easily expressed as integrals over impact parameter b :

$$\sigma_{\text{tot}}(s) = 2 \int d^2b \left[1 - \text{Re} \left(e^{-\chi(b, s)}\right)\right], \quad (2a)$$

$$\sigma_{\text{el}} = \int d^2b \left|1 - e^{-\chi(b, s)}\right|^2, \quad (2b)$$

$$\sigma_{\text{inel}} = \int d^2b \left(1 - \left|e^{-\chi(b, s)}\right|^2\right). \quad (2c)$$

Whereas σ_{tot} and σ_{el} depend on the real as well as the imaginary part of the eikonal, the inelastic cross section is determined by the real part of $\chi(b, s)$ alone.

There is ample experimental evidence that the inelastic nucleon-nucleon interactions can be divided into two classes, diffractive and nondiffractive events:

$$\sigma_{\text{inel}} = \sigma_{\text{D}} + \sigma_{\text{ND}}. \quad (3)$$

Following Durand and Pi, we assume that σ_{ND} can be calculated from perturbative QCD and the measured parton distributions, while σ_{D} is determined by soft strong interactions outside the domain of perturbative QCD. We thus make the assumption

$$\chi(b, s) = \chi_0(b, s) + \chi_{\text{QCD}}(b, s), \quad (4)$$

and we identify the real part of χ_{QCD} with the contribution of perturbative parton-parton scattering.

For the perturbative QCD contribution we have

$$\sigma_{\text{QCD}}(s) = \sum_{i, j} \int_0^1 dx_1 \int_0^1 dx_2 \int dt \frac{d\sigma_{ij}}{dt} f_i(x_1, Q^2) f_j(x_2, Q^2) \theta \left(Q^2 - (p_T^{\min})^2\right), \quad (5)$$

where f_i, f_j are the parton structure functions of the colliding hadrons (i and j are flavor indices) and $d\sigma_{ij}/dt$ are the parton-parton cross sections calculated in lowest order in

QCD [5]. A summation over different final state channels in the interaction of partons i, j is implicitly included in eq. (5).

In the impulse approximation $\text{Re } \chi(b, s)$ factorizes:

$$\text{Re } \chi(b, s) = \frac{1}{2} \sigma(s) A(b), \quad (6)$$

where the profile function $A(b)$ is related to the impact parameter distribution $\rho(b)$ of partons in the nucleon:

$$A(b) = \int d^2b' \rho(|\mathbf{b} - \mathbf{b}'|) \rho(b'). \quad (7)$$

It is well known [6] that the measured differential elastic nucleon cross section ($2b$) is well described by an eikonal based on the elastic form factor of the nucleon $G_E(k_\perp^2)$, corresponding to an exponentially decaying matter distribution with mean square radius $R_p = \sqrt{12}/\nu = 0.811$ fm. We assume that this distribution describes all parton flavors.

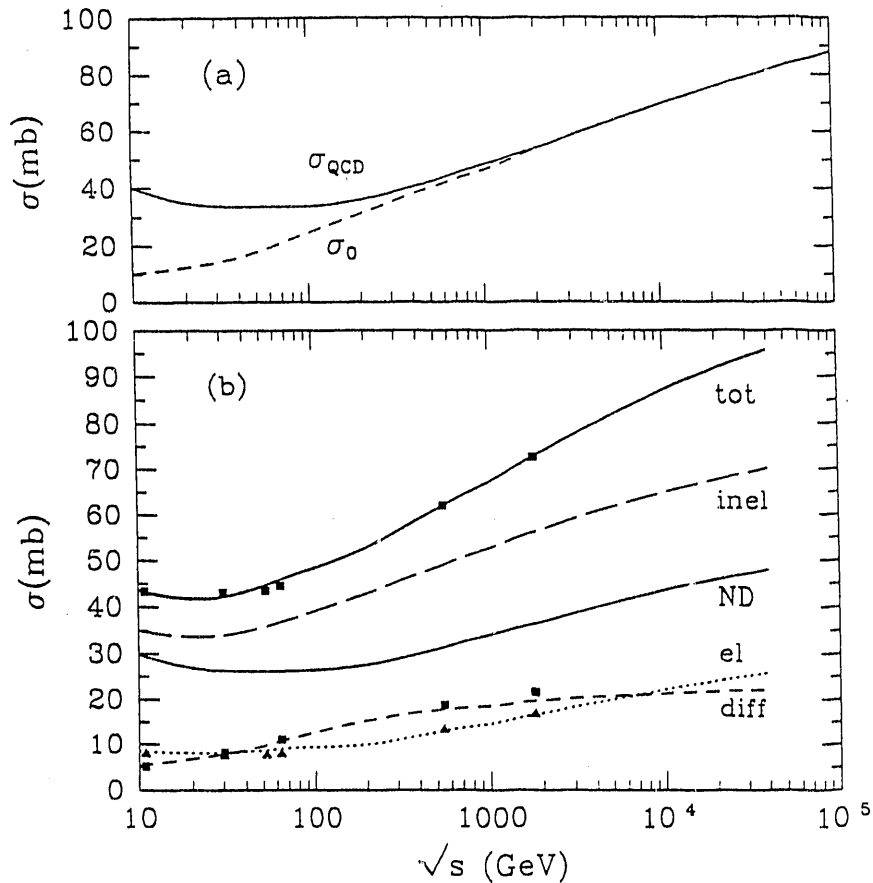


Fig. 1: (a) The eikonal QCD-cross section σ_{QCD} and eikonal diffractive cross section σ_0 obtained from the analysis of phenomenological fits for σ_{ND} and σ_{D} by means of eqs. (9, 10). The cross sections are set equal for $\sqrt{s} > 1.8$ TeV. (b) The total, inelastic, nondiffractive, elastic, and diffractive cross sections as obtained from σ_0 and σ_{QCD} by means of the eikonal representation. The points correspond to experimental data.

We have evaluated $\sigma_{\text{QCD}}(s)$ according to eq. (5) as a function of cut-off momentum p_T^{min} for two different sets of parton structure functions, those given by Eichten et al. [7] (EHLQ, set 1), and those obtained by Glück, Reya, and Vogt [8] (GRV h.o.), both with $\Lambda = 0.2$ GeV, where Λ is the QCD scale parameter. The eikonal cross sections $\sigma_{\text{QCD}}(s)$ and $\sigma_0(s)$ can now be deduced from σ_{ND} and σ_{D} by means of eqs. (9) and (10). The resulting curves are exhibited in Fig. 1. The value $\sigma_{\text{QCD}} + \sigma_0 \approx 50$ mb for c.m. energies below 100 GeV is in good agreement with previous determinations [2,3], but our analysis differs from those in that most of this value is attributed to parton-parton scattering. Whether this assignment is meaningful, depends on the size of the transverse momentum cut-off p_T^{min} required to obtain $\sigma_{\text{QCD}}(s)$.

The values in our analysis are shown in Fig. 2 for the EHLQ, as well as for the GRV structure functions. The "data" points correspond to the c.m. energies 43, 63, 100, 200, 540, and 1800 GeV, respectively, where we performed a detailed analysis. The straight lines shown in Fig. 2 are least-square fits to these points; as one notices, the functional relation $p_T^{\text{min}} = p_0(s/1 \text{ GeV})^\alpha$ provides a very good description. The parameters are $\alpha = 0.115$, $p_0 = 0.485$ GeV/c for EHLQ functions and $\alpha = 0.151$, $p_0 = 0.357$ GeV/c for the GRV parametrization. As already pointed out by Durand and Pi [2], the probability that a parton interaction with momentum transfer of 1 GeV/c leads to inelastic scattering is greater than 99.9 percent. The QCD coupling constant at $p_T^{\text{min}} \simeq 1$ GeV/c is of order $\alpha_s \approx 0.375$, so that a perturbative analysis may still yield qualitatively correct results. We stress that p_T^{min} must be regarded as a phenomenological parameter which describes in a way the screening of the QCD interaction at large distances.

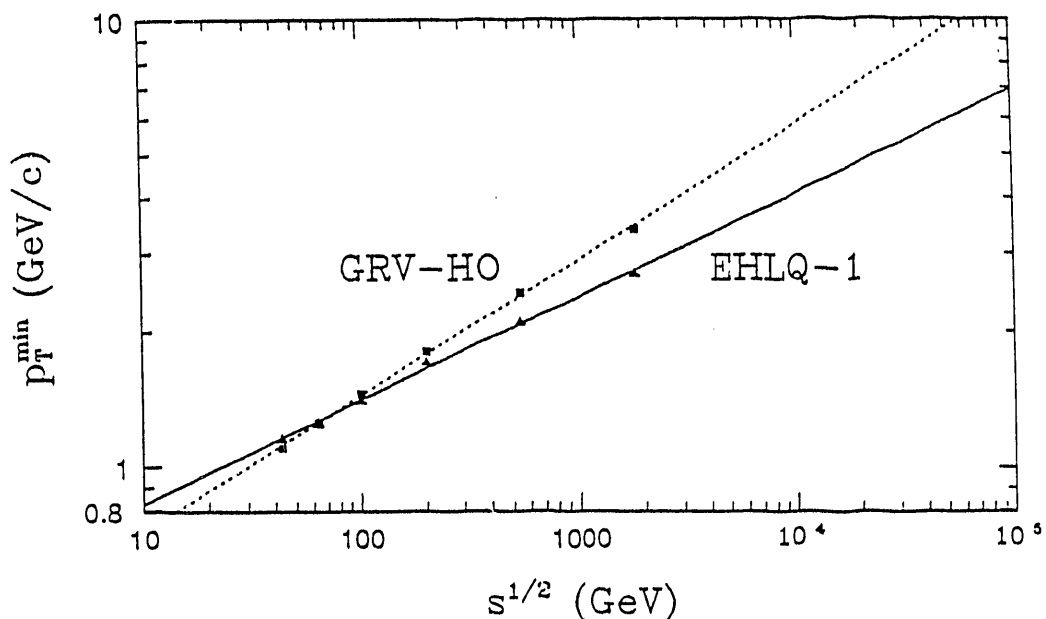


Fig. 2: The momentum cut-off p_T^{min} as obtained from the comparison with data, for EHLQ (set no. 1) and GRV (higher-order parametrization) structure functions. The points indicate where the detailed numerical analysis was performed. The straight lines represent least-square fits of the form $p_T^{\text{min}} = p_0 (s/\text{GeV})^\alpha$.

For energies corresponding to the specifications of RHIC we find that a momentum cut-off $p_T^{\min} = (1.75 \pm 0.1) \text{ GeV}/c$ is required to explain the nondiffractive cross section in terms of perturbative QCD interactions. This value is in good agreement with the findings of earlier studies. It is sufficiently large, to make a global description of nondiffractive hadronic scattering events in terms of parton cascades, with fragmentation governed by Altarelli-Parisi evolution a credible model.

- [*] N. Abou-El-Naga, K. Geiger, and B. Müller, *J. Phys. G*, in print.
- [1] T. Sjöstrand and M. van Zijl, *Phys. Rev. D* **36**, 2019 (1987).
- [2] L. Durand and H. Pi, *Phys. Rev. Lett.* **58**, 303 (1987) and *Phys. Rev. D* **40**, 1436 (1989).
- [3] T. K. Gaisser and F. Halzen, *Phys. Rev. Lett.* **54**, 1754 (1985).
- [4] M. Block, R. Fletcher, F. Halzen, B. Margolis, and P. Valin, *Phys. Rev. D* **41**, 978 (1990); M. M. Block, F. Halzen, and B. Margolis, *Phys. Lett.* **B252**, 481 (1990).
- [5] B. L. Combridge, J. Kripfganz, and J. Ranft, *Phys. Lett.* **B70**, 234 (1977).
- [6] T. T. Chou and C. N. Yang, *Phys. Rev.* **170**, 1591 (1968); A. W. Chao and C. N. Yang, *Phys. Rev. D* **8**, 2063 (1973).
- [7] E. Eichten, I. Hinchliffe, K. Lane, and C. Quigg, *Rev. Mod. Phys.* **56**, 579 (1984).
- [8] M. Glück, E. Reya, and A. Vogt, *Z. Phys.* **C48**, 471 (1990).

1.3. Probing Parton Thermalization Time with Charm Production

(B. Müller, X.N. Wang [*])

Hard or semihard parton scatterings with $p_T \geq 2 \text{ GeV}/c$ are expected to dominate the interaction mechanism [1,2] in relativistic heavy ion collisions at $\sqrt{s} \geq 100 \text{ AGeV}$. Those scattered partons, usually referred to as minijets, have been estimated to contribute a large fraction of transverse energy deposited in the central region of heavy ion collisions at BNL Relativistic Heavy Ion Collider (RHIC) and CERN Large Hadron Collider (LHC) energies. Because of their high density, the initially produced partons, mainly gluons, are expected to rescatter from each other leading to the suppression of high p_T jets [3] as well as to partial thermal and chemical equilibration in the dense partonic system.

The thermalization time of the dense matter due to parton cascading and bremsstrahlung is usually longer [4,5] than what has been otherwise estimated [6]. Unless there are some yet unknown nonperturbative mechanisms which drive the system more quickly into equilibrium, the dense partonic matter could hadronize before being thermalized. Therefore, it is of interest to have some observables whose values can be related to the thermalization time. We present arguments indicating that the total charmed quark production may be used for this purpose.

In general, we can divide the charm production into three stages: (1) initial production similar to minijets; (2) pre-equilibrium production from secondary parton cascade; (3) and thermal production. For a reasonable range of temperatures ($T \sim 200\text{--}400 \text{ MeV}$), the thermal production is far below the initial one [7] due to the heavy quark mass $M_c \approx 1.5 \text{ GeV}/c^2$. The charm production from the interaction between comovers in the hadronic phase should be even more suppressed for the same reason. On the other hand, secondary parton scatterings in the initially produced dense, though not thermalized, partonic system could lead to significant charmed quark production. The dominant process in this

pre-equilibrium stage is through gluon fusion. Due to the small interaction rate for $gg \rightarrow c\bar{c}$ relative to elastic gluon scattering $gg \rightarrow gg$, the chemical equilibrium time for the charmed quarks is much longer than the parton thermalization time. Therefore, the total number of charmed quarks produced in the pre-equilibrium stage should be approximately proportional to the thermalization time of the whole partonic system. When this pre-equilibrium charm production becomes comparable to, if not larger than, the initial production, the total charm can be used as a measure of the thermalization time scale. Another reason why the enhancement of hadrons with open charm is unique is that it is little influenced by final state interactions.

The number of hard or semihard parton scatterings in $A + B$ collisions is given via perturbative QCD as,

$$\frac{dN_{jet}(b)}{dp_T^2 dy_1 dy_2} = K \int d^2 \mathbf{r} \sum_{a,b} x_1 f_{a/A}(x_1, p_T^2, \mathbf{r}) x_2 f_{b/B}(x_2, p_T^2, \mathbf{b} - \mathbf{r}) \frac{d\sigma_{ab}}{d\hat{t}}, \quad (1)$$

where $d\sigma_{ab}$ is the cross section for parton-parton scatterings, y_1 and y_2 are the rapidities of the scattered partons, x_1 and x_2 are the light-cone momentum fractions carried by the initial partons, and the summation runs over all parton species. The factor $K \approx 2$ accounts for next-to-leading order effects. From deep inelastic lepton scattering on nuclei it is well known that the quark structure functions with small $x \leq 0.1$ are depleted in a nucleus relative to a free nucleon. This depletion, usually referred to as parton shadowing, is also expected for gluons. Although the present data on charm production in $p + A$ collisions can shed some light on this, we simply assume here that quarks and gluons are shadowed by the same amount.

Equation (1) can be used to calculate charm production in the initial parton scatterings. Taking into account of parton shadowing, we estimate the total number of charmed quark pairs in a central $Au + Au$ collision to be about 2 (34) at $\sqrt{s} = 200$ (6000) GeV. The A dependence of charm production per central event is $N_c \propto A^{4/3}$, neglecting parton shadowing. Since the density of initially produced partons, mainly gluons, is very high, they will inevitably rescatter from each other leading to partial thermalization as well as charm production. Given the phase space density of the initially produced gluons $f(k)$, the differential production rate is then

$$E \frac{d^3 A}{d^3 p} = \frac{1}{(2\pi)^8} \int \frac{d^3 k_1}{\omega_1} \frac{d^3 k_2}{\omega_2} f(k_1) f(k_2) \delta^{(4)}(k_1 + k_2 - p - p_2) \frac{1}{2} g_G^2 \pi \hat{s}^2 \frac{d\sigma_{gg \rightarrow c\bar{c}}}{d\hat{t}} \frac{d^3 p_2}{E_2}, \quad (2)$$

The initial phase space density for gluons can be related to $dN_{jet}/dk_T dy$ as calculated from Eq. (1) by

$$f(k) = \frac{(2\pi)^2}{g_G V} \frac{1}{k_T |\mathbf{k}|} \frac{dN_{jet}}{dk_T dy} \equiv \frac{(2\pi)^2}{g_G V} g(k), \quad (3)$$

where V is the volume of the partonic system. In our actual calculation we have used the results of the HIJING Monte Carlo model [2] for $dN_{jet}/dk_T dy$ in which initial and final

state radiation is also included. To obtain an order of magnitude estimate, we neglect the time evolution of the distribution $g(k)$ and assume that it remains unchanged during the thermalization time τ_0 .

If the complicated expansion of the partonic system during τ_0 is taken into account, the dependence of Ed^3N_c/d^3p on τ_0/τ_i will change and is model dependent, but the fact that it increases with τ_0/τ_i remains. Since $g(k)$ is proportional to $A^{4/3}$, we can see that the pre-equilibrium charm production grows like A^2 as compared to $A^{4/3}$ for the initial production. The energy dependence is also much stronger since $g(k_1)g(k_2)$ is proportional to σ_{jet}^2 .

The thermal production of charmed quarks is completely analogous to that of strange quarks which has been studied extensively. We refer to [8] for details. In our calculation, we follow the idealized scaling hydrodynamic expansion of QGP with phase transition temperature $T_C = 160$ MeV.

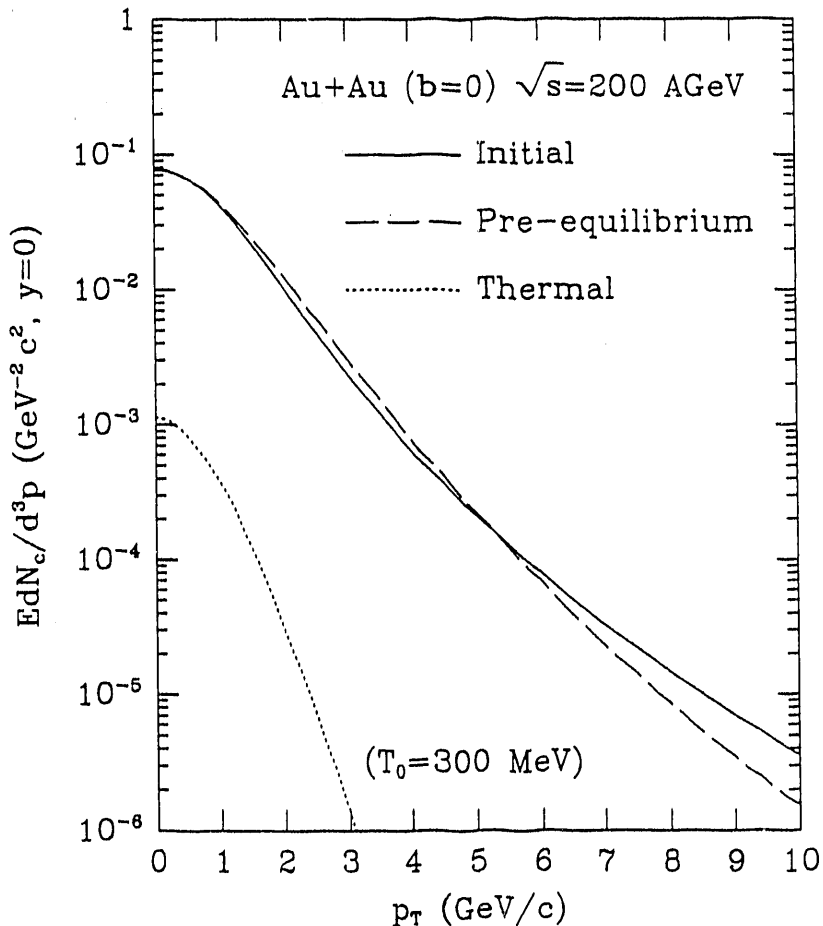


Fig. 1: The p_T distribution of initial (solid), pre-equilibrium with $\tau_0 = 1$ fm/c (dashed), and thermal (dotted) charm production in central $Au + Au$ collisions at $\sqrt{s} = 200$ GeV.

Shown in Fig. 1 are the transverse momentum distributions of charm production in central $Au + Au$ collisions at $\sqrt{s} = 200$ AGeV. For the pre-equilibrium production (dashed

line), we have assumed the initial parton production time $\tau_i = 0.1$ fm/c and the thermalization time $\tau_0 = 1$ fm/c. It almost looks identical to the initial direct charm production (solid line), except that its spectrum at large p_T is softer indicating the partial thermalization due to parton cascading. For the initial temperature $T_0 = 300$ MeV, thermal charm production (dotted line) is negligible as compared to initial and pre-equilibrium production.

Due to gluon shadowing the ratio $R_{AB}^c = \sigma^{AB}/AB\sigma^{pp}$ for the initial charm production at low $p_T = 1$ GeV/c as shown in Fig. 2 (dashed line) is only about 0.5 for central $Au + Au$ collisions at $\sqrt{s} = 200$ AGeV. However, if the pre-equilibrium contribution with $\tau_0 = 1$ fm/c is included (solid line) the ratio becomes about 1 in the central rapidity region. At $\sqrt{s} = 6000$ AGeV, the shadowing suppresses the initial production by 2/3 (dotted line) and the pre-equilibrium production is so abundant that it increases the ratio R_{AB}^c to 1.7 even though we have assumed a very short thermalization time of $\tau_0 = 0.3$ fm/c.

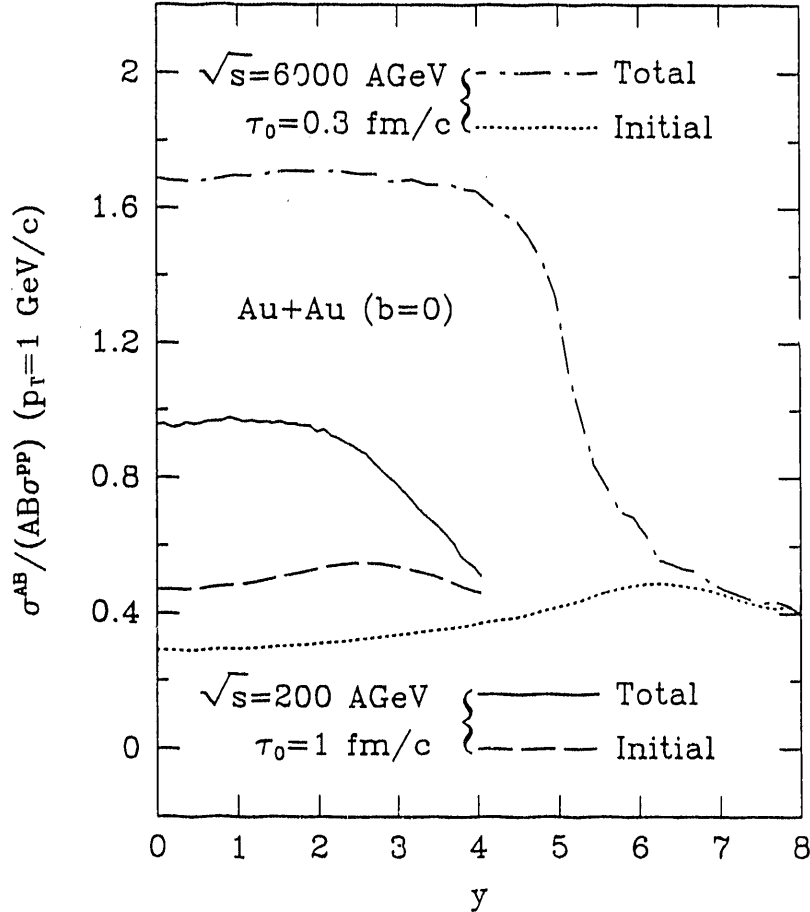


Fig. 2: The ratio $R_{AB}^c = \sigma^{AB}/AB\sigma^{pp}$ for charm production at $p_T = 1$ GeV/c as functions of rapidity in central $Au + Au$ collisions at $\sqrt{s} = 200$ (6000) GeV. The solid (dotdashed) line is for the total charm with thermalization time $\tau_0 = 1$ (0.3) fm/c while the dashed (dotted) line is only for the initial production.

The pre-equilibrium enhancement over the initial charm production depends sensitively on the value of thermalization time τ_0 . This demonstrates that the total charm

production can be used as a measure of the thermalization time scale. We also note that the pre-equilibrium enhancement is only relative to the suppression by gluon shadowing. Since gluon shadowing is also a fundamental issue in its own right, it is therefore essential to study the charm production systematically in $p + p$ and $p + A$ collisions at the same energy where the only nuclear effect comes from gluon shadowing. Unlike J/Ψ which can be absorbed by the nuclear matter, open charm production in $p + A$ is not influenced by final state interactions. It is therefore unique and useful for determining gluon shadowing which in turn can be used to extract information on pre-equilibrium charm enhancement and jet quenching in $A + A$ collisions.

- [*] B. Müller and X.-N. Wang, Phys. Rev. Lett. **68**, 2437 (1992).
- [1] K. Kajantie, P.V. Lardshoff and J. Lindfors, Phys. Rev. Lett. **59**, 2517 (1987); K.J. Eskola, K. Kajantie and J. Lindfors, Nucl. Phys. **B323**, 37 (1989).
- [2] X.-N. Wang and M. Gyulassy, Phys. Rev. **D44**, 3501 (1991).
- [3] X.-N. Wang and M. Gyulassy, preprint Duke-TH-91-25/LBL-31619 (1991).
- [4] K. Geiger and B. Müller, Nucl. Phys. **B369**, 600 (1992).
- [5] K.J. Eskola, K. Kajantie, and J. Lindfors, Phys. Lett. **B214**, 613 (1988).
- [6] R.C. Hwa and K. Kajantie, Phys. Rev. Lett. **56**, 696 (1986).
- [7] J. Cleymans and R. Philippe, Z. Phys. **C22**, 271 (1984); H.-J. Reusch, Z. Phys. **C26**, 105 (1984).
- [8] P. Koch, B. Müller, and J. Rafelski, Phys. Rep. **142**, 167 (1986); T. Matsui, B. Svetitsky, and L.D. McLerran, Phys. Rev. D **34**, 2047 (1986).

1.4. Color Screening in Relativistic Heavy Ion Collisions

(T.S. Biró, B. Müller, X.N. Wang [*])

The physical processes occurring at very early times ($\tau \ll 1\text{fm}/c$) in violent collisions between heavy nuclei are probably best described in the framework of perturbative quantum chromodynamics (PQCD). It is an interesting question whether those processes, which can be adequately treated by PQCD, can lead to the formation of a locally thermalized system of quarks and gluons, the quark-gluon plasma. Such a thermalization scenario, which has been discussed in the context of the QCD parton model [1-3], would be in contrast to the often advocated model of independent flux-tubes or strings [4]. In order to explore, whether there can exist a pre-equilibrium stage in string formation governed by non-perturbative physics, we have calculated the color screening length in a dense medium of quarks and gluons produced by semi-hard QCD interactions among partons in colliding nuclei. Our analysis is based on the HIJING Monte Carlo code [5], which models the earliest stage of the nuclear collision as Glauber-type superposition of independent parton interactions determined by PQCD.

Because gluon-gluon scattering is by far the dominant semihard process in hadronic interactions, most of the perturbatively scattered and radiated partons are gluons. We have, therefore, neglected the influence of quarks on the screening of color forces between scattered partons. In Coulomb gauge we obtain the following expression for the screening mass of the timelike gluon propagator,

$$m^2 = -\frac{3\alpha_s}{\pi^2} \lim_{|q| \rightarrow 0} \int d^3k \frac{|\mathbf{k}|}{\mathbf{q} \cdot \mathbf{k}} \mathbf{q} \cdot \nabla_{\mathbf{k}} f(\mathbf{k}), \quad (1)$$

where α_s is the strong coupling constant and $f(\mathbf{k})$ is the phase space density of gluons. The Debye screening length of the force between static color charges is given by $\lambda = 1/m$. Because the gluon distribution will initially be anisotropic with respect to the beam axis, the screening mass of a propagating gluon depends on its direction with respect to that axis.

Assuming a central plateau in the multiplicity distribution, we write

$$g(k_T, y) = \frac{2(2\pi)^2}{g_G V} \frac{1}{|\mathbf{k}|} \frac{1}{2Y} g(k_T) [\theta(y + Y) - \theta(y - Y)] \quad (2)$$

and determine the transverse momentum distribution $g(k_T) = dN_G/dk_T^2$ by comparison with the HIJING results. The final expressions for the transverse and longitudinal gluon screening mass are then:

$$m_T^2 = \frac{3\alpha_s}{\tau_i R_A^2} \frac{\sin^{-1}(\tanh Y)}{Y} \int dk_T g(k_T),$$

$$m_{||}^2 = m_T^2 \left[1 + \frac{1}{\sinh Y \sin^{-1}(\tanh Y)} \right]. \quad (3)$$

Here τ_i characterizes the formation time for the initially produced gluons and R_A is the nuclear radius of the colliding nuclei. Using the uncertainty principle argument, we take the formation time to be $\tau_i = 1/\langle k_T \rangle$ and $\langle k_T \rangle$ is the average transverse momentum of the produced gluons. Since the total number of produced partons is proportional to the number of binary nucleon-nucleon interactions, $g(k_T)$ has roughly a nuclear dependence of A^2 . Therefore, the screening mass grows as $A^{2/3}$. At high energies, $m_{||}$ is very close to m_T .

With the input of the HIJING predictions of initially produced gluon distribution we obtain the following values of the screening length for central $Au + Au$ collisions,

$$\begin{aligned} \lambda_{||} &= 0.38 \text{ fm}, & \lambda_T &= 0.4 \text{ fm} & (\text{RHIC}), \\ \lambda_{||} &= 0.13 \text{ fm}, & \lambda_T &= 0.13 \text{ fm} & (\text{LHC}), \end{aligned} \quad (4)$$

where we have used the value $\alpha_s = 0.3$. The values predicted for LHC energy are small due to the very high density of initially scattered gluons at this energy. They indicate that one cannot expect the formation of extended coherent color field configurations, such as color flux-tubes with a radius of about 0.5 fm. in such an environment. Color forces will be screened before nonperturbative infrared aspects of QCD set in. The situation at RHIC energies is somewhat ambiguous since the screening length is not much smaller than the radius of an independent flux-tube. However, as compared to the estimate of the screening mass in thermal QCD, $1/m_{\text{th}} \approx 0.36 \text{ fm}$ at $T = 200 \text{ MeV}$ and $\alpha_s = 0.6$, it is still not unlikely that a quark-gluon plasma could be created directly from the rescattering of the gluons initially produced in semihard collisions.

[*] T.S. Biró, B. Müller, X.N. Wang, preprint DUKE-TH-92-26, Phys. Lett. B (in print).

[1] R. Hwa and K. Kajantie, Phys. Rev. Lett. 56, 695 (1986).

- [2] J. P. Blaizot and A. H. Mueller, Nucl. Phys. B **289**, 847 (1987).
- [3] K. Geiger and B. Müller, Nucl. Phys. B **369**, 600 (1992) .
- [4] See e.g.: T. Matsui, Nucl. Phys. A **461**, 49c (1987).
- [5] X.-N. Wang and M. Gyulassy, Phys. Rev. D **44**, 3501 (1991).

2. MINIJETS IN HADRONIC AND NUCLEAR COLLISIONS

2.1. Minijets or QGP in $p\bar{p}$ High Energy Collisions?

(X.-N. Wang, M. Gyulassy [*])

In hydrodynamic models transverse collective flow is usually generated from the expansion of the thermalized dense system [1]. Since all hadrons have the same flow velocity, heavy particles tend to have larger transverse momentum when they finally freeze out. If the average transverse momentum is plotted against the total multiplicity, it is anticipated that for heavy particles it will be larger and the increase with the multiplicity will be faster than for light ones. Quite surprisingly, experiments on $p\bar{p}$ collisions at Tevatron Collider energy have recently reported observation of just this effect [2]. Lévai and Müller [3] have recently studied this reaction and indicated that a QGP might have been formed. However the common transverse flow of hadrons may also arise accidentally from the fragmentation of minijets. This is the possibility that we explore in detail here. We show that the observed transverse flow effect does in fact arise naturally from the fragmentation of multiple minijets.

Our focus in this letter is on the effects of the production and fragmentation of minijets which are simply the *non-equilibrium* moderate $p_T \geq 2$ GeV/c partons produced copiously at high energies in perturbative QCD (PQCD). Our study is based on a newly developed (HIJING) Monte Carlo model [4] which combines low p_T string phenomenology with PQCD for high p_T processes and is consistent with a variety of data over a wide energy range in high energy pp and $p\bar{p}$ collisions. The basic assumption in this model is independent multiple minijet production. The cross sections for no and $j \geq 1$ number of jet productions with $p_T \geq p_0$ are,

$$\begin{aligned}\sigma_0 &= \int d^2b [1 - e^{-\sigma_{soft} T_N(b,s)}] e^{-\sigma_{jet} T_N(b,s)}, \\ \sigma_j &= \int d^2b \frac{[\sigma_{jet} T_N(b,s)]^j}{j!} e^{-\sigma_{jet} T_N(b,s)}.\end{aligned}\quad (1)$$

Their sum gives rise to the total inelastic cross section σ_{in} . In the above equations, $\sigma_{jet}(p_0)$ is the total inclusive jet cross section with $p_T \geq p_0$ calculated via PQCD, σ_{soft} is the phenomenological inclusive cross section for soft interactions and $T_N(b,s)$ is the partonic overlap function between two nucleons at impact parameter b which we approximate by using the Fourier transform of a dipole form factor as the partonic density for each nucleon [5].

Shown in Fig.1 is our calculated result on the correlation between $\langle p_T \rangle$ and the total charged multiplicity n_{ch} for different hadrons. The average p_T is obtained by applying the same procedure as used in the experiment [2] in which the p_T distributions are first fitted with parametrizations (power law $a(p_T + b)^{-n}$ for pions and exponential $\beta \exp(-\alpha p_T)$ for kaons and antiprotons) and then the fitted parameters are used to calculate $\langle p_T \rangle$ in the restricted range $0 < p_T < 1.5$ GeV/c. For all hadrons, $\langle p_T \rangle$ increases with n_{ch} . We also show as dashed lines in Fig. 2 our calculated results for pp collisions at RHIC energy, $\sqrt{s} = 200$ GeV. They are similar to the results at $\sqrt{s} = 1.8$ TeV, except that pions have

lower saturated value of $\langle p_T \rangle$ at RHIC energy. Since pions are the dominant produced particles, the high multiplicity $\langle p_T \rangle$ for all charged hadrons at $\sqrt{s} = 200$ GeV is smaller than at $\sqrt{s} = 1.8$ TeV.

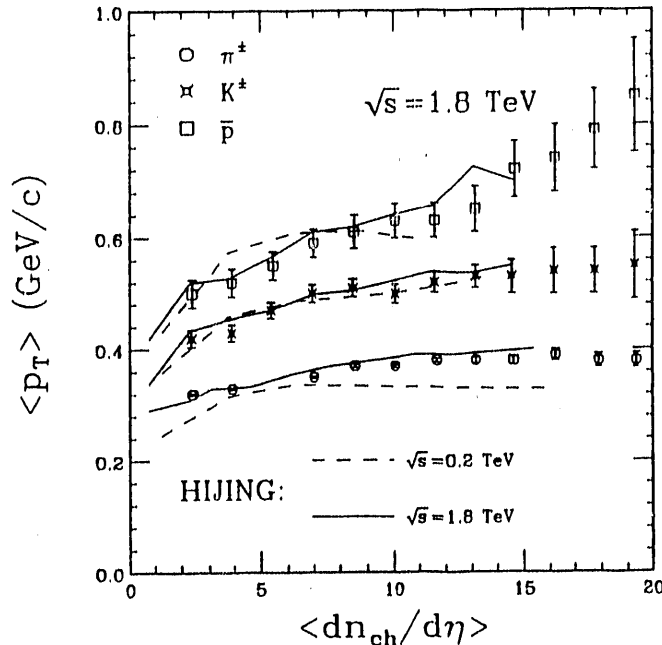


Fig. 1: $\langle p_T \rangle$ of pions, kaons, and anti-protons (from bottom to top) in $-0.36 < \eta < 1.0$ versus $dn_{ch}/d\eta$ in $|\eta| < 3.25$. The dashed lines are for pp collisions at $\sqrt{s} = 200$ GeV.

In a model with multiple minijet production, it is easy to understand why $\langle p_T \rangle$ increases with n_{ch} . If we decompose the multiplicity distribution into different contributions from events with different number of minijets, we find [4,6] that large multiplicity events are dominated by multiple minijet production while low multiplicity events are dominated by those of no jet production. At $\sqrt{s} = 1.8$ TeV, the average number of individual minijets in $p\bar{p}$ is only about two, but on rare occasions up to ten partons with $p_T > 2$ GeV/c are produced over the whole rapidity interval. In this sense, the produced nonequilibrium partonic system is quite tenuous in $p\bar{p}$ collisions. Nevertheless, those few partons are enough to explain the increase of the average transverse momentum with n_{ch} . In order to understand the different behavior of the correlation between $\langle p_T \rangle$ and n_{ch} for different particles, we recall that the jet fragmentation functions for heavy hadrons tend to be harder as measured in e^+e^- annihilation experiments [7]. Therefore, heavy hadrons from jet fragmentation carry larger transverse momentum than the light hadrons in pp or $p\bar{p}$ collisions as well. This leads naturally to the larger slopes of $\langle p_T \rangle$ vs n_{ch} correlation for heavier particles. Since the mass difference between Λ and \bar{p} is very small, we find that n_{ch} dependence of $\langle p_T \rangle$ for the two are almost the same in agreement with the recent data [8].

In conclusion, we emphasized here that multiple minijet production and fragmentation provide a natural explanation for the apparent transverse flow phenomena observed in $p\bar{p}$ reactions without having to resort novel quark-gluon plasma (QGP) mechanisms.

- [*] X.-N. Wang and M. Gyulassy, Transverse Flow due to Minijets in $p\bar{p}$ Collisions at $\sqrt{s} = 1.8$ TeV, Duke-Th-91-24, Phys. Lett. B in press.
- [1] G. Baym, B. L. Friman, J. P. Blaizot, M. Soyeur, and W. Czyz, Nucl. Phys. **A407**, 541(1983); M. Kataja, P. V. Ruuskanen, L. D. McLerran, and H. von Gersdorff, Phys. Rev. D **34**, 2755(1986); X.-N. Wang and R. C. Hwa, Phys. Rev. D **35**, 3409(1987).
- [2] T. Alexopoulos, et al., Phys. Rev. Lett. **64**, 991(1990).
- [3] P. Lévai and B. Müller, Phys. Rev. Lett. **67**, 1519(1991).
- [4] X.-N. Wang and M. Gyulassy, Phys. Rev. D **44**, 3501 (1991).
- [5] X.-N. Wang, Phys. Rev. D **43**, 104 (1991).
- [6] X.-N. Wang and M. Gyulassy, Phys. Rev. D **45**, 844 (1992).
- [7] S. L. Wu, Phys. Rep. **107**, 59(1984).
- [8] T. Alexopoulos, et al., preprint Duke-HEP-91-11. The lambda to antiproton ratio of 0.39 in this paper is used to normalize the lambda p_T distribution in Fig. 2.

2.2. Resolving Minijets in Hadronic Interactions

(X.-N. Wang [*,**])

We have learnt that the observed multiplicity and mass dependence of the average transverse momentum [1] in high energy hadronic collisions can naturally arise from minijet production [2]. However, minijets are difficult to resolve as distinct jets from the background when one uses the conventional cluster-finding method [3]. Due to this lack of direct experimental evidence of minijet production, it is hard to disprove the possibility that the phenomenon could also come from the transverse flow of an expanding quark gluon plasma or string interaction [4]. In order to differentiate the minijet picture from the other scenarios, the study of some new observables characteristic of minijets are obviously necessary.

We propose here that the p_T dependence of two-particle correlation function can be utilized to study the minijet content in the minimum biased events of hadronic interactions. Because particles from jet fragmentation tend to cluster together in phase space, two-particle correlation must be enhanced due to minijet production. Especially for two-particle correlation in the azimuthal angle ϕ , contribution from back-to-back minijets should be strongly peaked at both forward ($\Delta\phi = 0$) and backward ($\Delta\phi = \pi$) directions. If we calculate the same correlation, but for some selected particles whose transverse momenta are larger than a certain p_T cut, the two peaks should be more prominent because these particles are more likely to come from minijets. On the contrary, particles from soft production or an expanding quark gluon plasma are isotropical in the transverse plane and would only have some nominal correlation in the backward direction due to momentum conservation.

It is well known that particles from high p_T jets are very concentrated in both directions of the back-to-back jets. The widths of these high p_T jet profiles are about 1 in both pseudorapidity η and azimuthal angle ϕ [5]. Minijets, though with smaller p_T , should have similar properties. We will study the two-particle correlation functions of the produced particles in the minimum biased events and their p_T dependence. Since particles with $p_T > p_T^{cut}$ are more likely to come from jet fragmentation, we can expect that the two-particle correlation functions are more characteristic of jet profiles when p_T^{cut} is larger.

Let us consider two-particle correlation in the azimuthal angle ϕ first. The normalized two-particle correlation functions are defined as

$$c(\phi_1, \phi_2) = \frac{\rho(\phi_1, \phi_2)}{\rho(\phi_1)\rho(\phi_2)} - 1, \quad (1)$$

where $\rho(\phi)$ is the averaged particle density in ϕ and $\rho(\phi_1, \phi_2)$ is the two-particle density which is proportional to the probability of joint particle production at ϕ_1 and ϕ_2 .

Shown in Fig. 1 are our calculated results, using HIJING Monte Carlo model, on two-particle correlation functions in $p\bar{p}$ collisions at $\sqrt{s} = 1.8$ TeV for selected particles with different p_T cut. The calculation includes all charged particles in the full rapidity range. As we have expected, due to minijets, there is strong two-particle correlation at both $\Delta\phi = 0$ and π , forming a valley at $\Delta\phi \sim \pi/3$. For large p_T^{cut} , the correlation functions are very similar to large p_T jet profiles as functions of ϕ relative to the triggered jet axis [5]. These features are, however, absent in low energy hadronic collisions where minijet production is negligible. Since there are still many particles from soft production which can contribute only to backward correlation due to momentum conservation, the study of energy dependence of the relative height of the two peaks at $\Delta\phi = 0$ and π could provide us information about the energy dependence of minijet production. The background at $\Delta\phi \sim \pi/3$ also depends on the average number of minijet production.

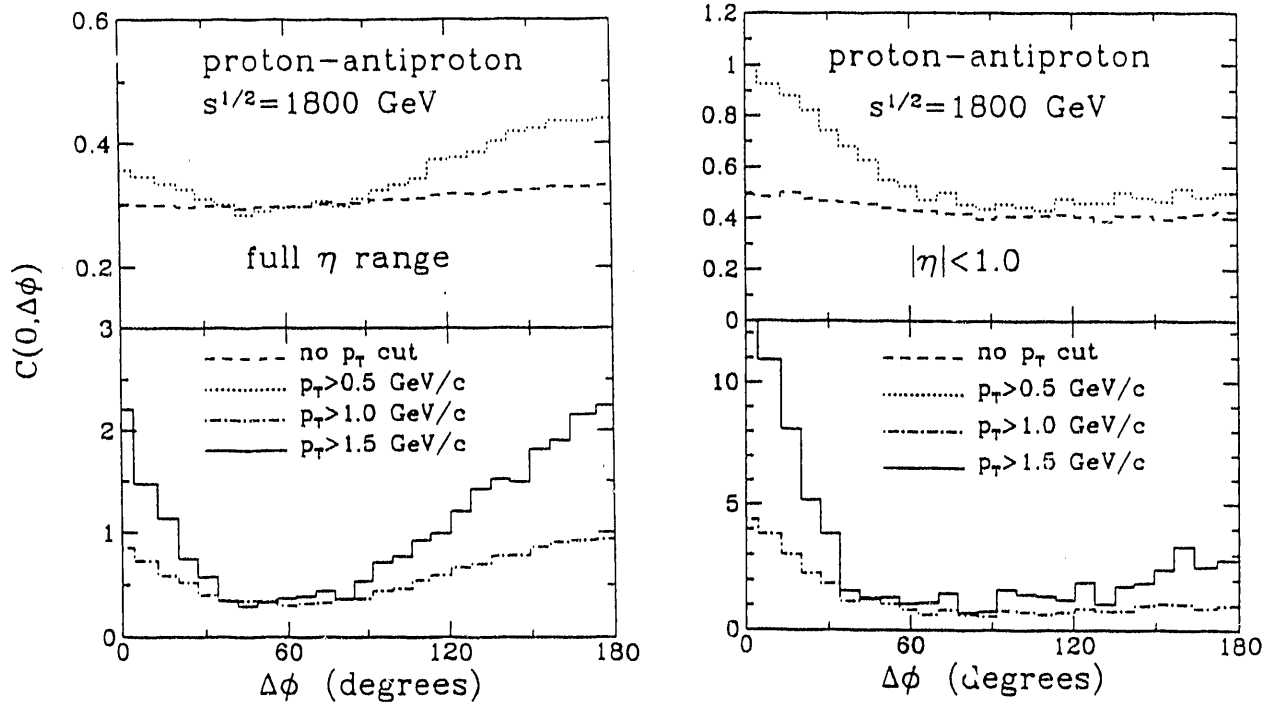


Fig. 1: (a) $c(0, \Delta\phi)$ vs $\Delta\phi$ between two charged particles in the full rapidity range. The dashed line is for all charged particles, dotted line for particles with $p_T > 0.5$ GeV/c, dash-dotted line for $p_T > 1.0$ GeV/c, and solid line for $p_T > 1.5$ GeV/c. (b) The same as (a), except for charged particles in a limited rapidity range of $|\eta| < 1$.

Unlike high p_T back-to-back jets which are both kinematically bounded to the central rapidity region, a pair of minijets can be easily produced with large rapidity gap between them. When we trigger one minijet in a limited rapidity window, the other one which is produced in the same parton scattering often falls outside the rapidity window. Therefore, if we calculate two-particle correlation for particles in a limited rapidity range, minijet contribution to the backward correlation ($\Delta\phi = \pi$) will mostly drop out while the contribution to forward correlation ($\Delta\phi = 0$) still remains. Indeed, as shown in Fig. 2, the forward correlation at $\Delta\phi = 0$ for particles in $|\eta| < 1$ is very strong, but the backward correlation at $\Delta\phi = \pi$ is drastically reduced as compared to the correlation pattern in the full rapidity range in Fig. 1. Furthermore, due to strong short range two-particle correlation in rapidity [6], the forward correlation at $\Delta\phi = 0$ is also enhanced by restricting particles to $|\eta| < 1$. At $\sqrt{s} = 1.8$ TeV, we find that the enhancement of backward correlation at $\Delta\phi = \pi$ due to minijets becomes important only when the rapidity window is $|\eta| \geq 2$.

To conclude, we have proposed and demonstrated that two-particle correlation functions in azimuthal angle ϕ and rapidity η and their p_T dependence can be used to resolve minijet contribution to particle production in minimum biased hadronic interactions. It is especially important to test this experimentally so as to reveal the real mechanism for the observed multiplicity and mass dependence of the average transverse momentum.

- [*] X.-N. Wang, Resolving Minijets in the Minimum Biased Events of Hadronic Interactions, submitted to Phys. Rev. D.
- [**] X.-N. Wang, Studying Minijets via the p_T Dependence of Two-particle Correlations in ϕ , submitted to Phys. Rev. D.
- [1] T. Alexopoulos, *et al.*, Phys. Rev. Lett. **64**, 991 (1990).
- [2] X.-N. Wang and M. Gyulassy, Duke preprint, DUKE-TH-91-24, Phys. Lett. **B**, in press.
- [3] A. Byon, CDF Ph.D. thesis, Purdue University.
- [4] C. Merino, C. Pajares, and J. Ranft, Phys. Lett. **276B**, 168 (1992).
- [5] T. Akesson *et al.* (AFS Collaboration), Z. Phys. C **30**, 27 (1986); and the reference therein.
- [6] X.-N. Wang and M. Gyulassy, Phys. Rev. D **45**, 844(1992), and the references therein.

2.3. Gluon Shadowing and Jet Quenching in High Energy $A + A$ Collisions (X.-N. Wang, M. Gyulassy [*])

If minijets are important in high energy hadronic interactions, they must also play a major role in ultrarelativistic heavy ion collisions. In this letter we emphasize two novel nuclear effects on multiparticle production in $A + A$ as predicted by HIJING for $\sqrt{s} \geq 200$ AGeV due to (1) gluon shadowing [1] and (2) jet quenching [2]. From deep inelastic scatterings [3], it is well known that the quark structure functions with small $x \leq 0.1$ fractional momenta are depleted in a nucleus relative to a free nucleon. This depletion, usually referred to as nuclear shadowing, is also expected for the gluon structure function although there is no clear experimental evidence for that yet. Gluon shadowing is of interest in high energy nucleus-nucleus collisions because it could influence significantly the initial conditions in such reactions. In addition, it is of fundamental interest in its own right as it pertains to the nuclear structure at the parton level not accessible via deep

inelastic reactions. Jet quenching, on the other hand, is of interest because it provides information on the final state interaction processes that may lead to partial thermal and chemical equilibration in the produced dense partonic system. Jet quenching results from the energy loss, $dE/d\ell$, of a high p_T parton as it traverses the dense matter. PQCD estimates [4] indicate that induced gluon bremsstrahlung may dominate the energy loss mechanism and that $dE/d\ell \propto \alpha_s \mu_D^2 \log^2(E/\mu_D) \sim 1-3$ GeV/fm depends sensitively on the infrared (Debye) screening scale μ_D of the medium. Jet quenching therefore provides information on that interesting scale, which may vary significantly in the vicinity of the quark-gluon plasma transition.

To test the sensitivity of minijet and particle production to gluon shadowing, we consider the possibility that both quarks and gluons are shadowed by the same amount in small x region. Motivated by geometrical considerations and constrained by EMC data [3], we parameterize the impact parameter dependent parton structure functions in a nucleus as

$$\frac{f_A(x)}{Af_N(x)} = 1 - a(x)(A^{1/3} - 1)\frac{4}{3}(1 - r^2/R_A^2)^{1/2}, \quad (1)$$

where $a(x) \approx 0.1 \exp(-x^2/0.01)$ describes the behavior of parton depletion at small $x \leq 0.1$, R_A is the nuclear radius and r is the transverse position of the parton's parent nucleon relative to the nuclear center.

Jet quenching in HIJING is implemented by a simplified gluon splitting algorithm to simulate induced gluon radiation [4]. The transverse coordinates of interaction points are determined assuming a cylindrical geometry and a constant mean free path λ_s . If $\Delta\ell$ is the distance between two interaction points, the total radiated energy is then estimated to be $\Delta E = \Delta\ell dE/d\ell$. While this jet quenching mechanism is obviously very schematic, it is sufficient in order to estimate the order of magnitude of the effects that are likely to result from final state interactions.

The calculated results for central $Au + Au$ collisions at $\sqrt{s} = 200$ AGeV are shown in Fig. 1. The left panel shows the pseudorapidity distributions of charged particles. Note that without minijets (dotted), the $2A$ soft beam jets in our model lead to $dN_{AA}/d\eta \approx AdN_{pp}/d\eta$. Each beam jet contributes about 0.75 to the central rapidity density almost independent of energy. Without gluon shadowing (dash-dotted), minijets are found to approximately triple the rapidity density due to beam jets. However, if gluon shadowing is of the same magnitude as that for quarks and antiquarks, then the minijet contribution to the rapidity density is reduced by approximately a half (dashed). The solid histogram shows that the effect of jet quenching on the rapidity density is small for $dE/d\ell = 2$ GeV/fm and $\lambda_s = 1$ fm.

In the middle panel of Fig. 1, we plot the ratio,

$$R^{AB}(p_T) = \frac{d^2 N_{AB}/dp_T^2/d\eta}{d^2 N_{pp}/dp_T^2/d\eta}, \quad (2)$$

of the inclusive p_T spectrum of charged particles in central $Au + Au$ collisions to that of $p + p$. For $p_T > 2$ GeV/c, both shadowing and quenching are seen to reduce dramatically the inclusive hadron production. In the absence of shadowing and jet quenching (dash-dotted) the ratio approaches the number of binary pp collisions in the reaction. Shadowing

alone (dashed) suppresses moderate p_T hadrons by a factor of about 2. Inclusion of jet quenching with $dE/d\ell = 2$ GeV/fm reduces that yield by another factor of about 3–5. It is remarkable and encouraging that the *single* inclusive hadron spectrum appears so sensitive to nuclear effects on jet production. Clearly higher order correlations, e.g. high p_T back-to-back hadron pairs, will be even more sensitive to these effects.

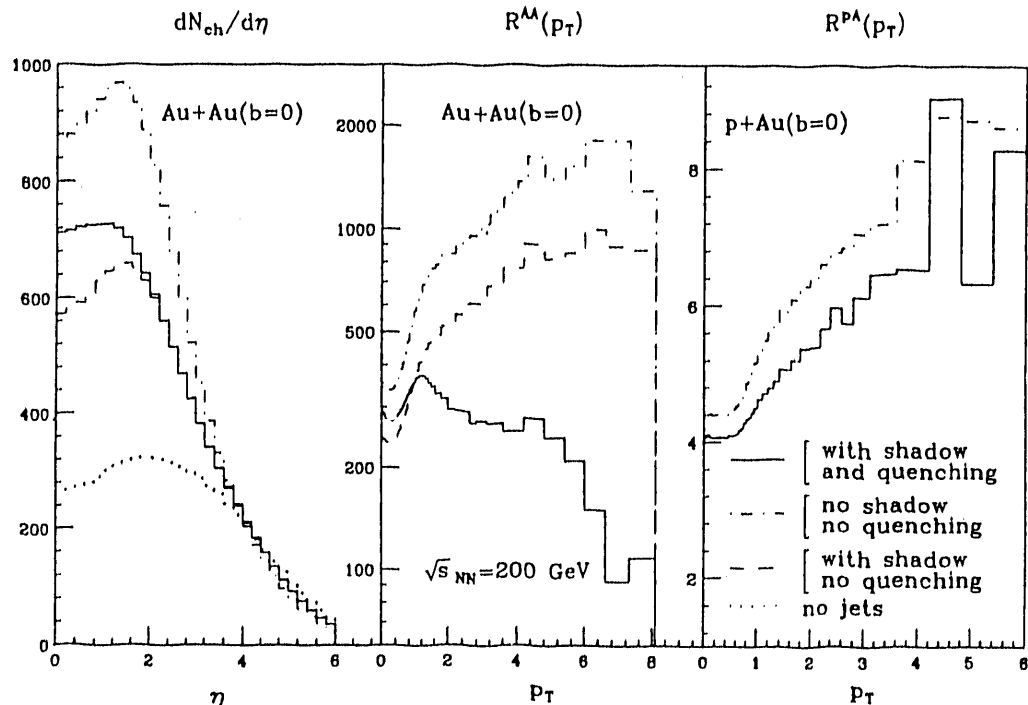


Fig. 1: Results of HIJING on the dependence of the inclusive charged hadron spectra in central $Au + Au$ and $p + Au$ collisions on minijet production (dash-dotted), gluon shadowing (dashed), and jet quenching (solid) assuming that gluon shadowing is identical to that of quarks and $dE/d\ell = 2$ GeV/fm with $\lambda_s = 1$ fm. $R^{AB}(p_T)$ is the ratio of the inclusive p_T spectrum of charged hadrons in $A + B$ collisions to that of $p + p$.

From the above, however, we see that $A + A$ data alone would not be sufficient to disentangle the effects of shadowing and jet quenching. To separate the two, $p + A$ collisions *must* be studied at the same energy! In those reactions, the density of comoving hadrons is so low that final state interactions leading to jet quenching should be negligible. Therefore, any observed suppression of moderate p_T hadrons could be attributed to gluon shadowing alone. The right panel in Fig. 1 shows the ratio as defined in Eq. (2) for central $p + Au$ collisions. Without shadowing (dash-dotted), the high p_T limit again reaches the number of binary collisions, which is about 8 in this case. The low p_T limit is, on the other hand, controlled by the number of *pairs* of beam jets, which is approximately 4 in central collisions. We see from this figure that the ratio $R^{pA}(p_T)$ at moderate p_T is indeed sensitive to gluon shadowing. Therefore, a systematic measurement of the inclusive hadron spectra in $p + p$ and $p + A$ at the same energy is essential in order to determine the magnitude of gluon shadowing. Once the magnitude of gluon shadowing is determined, its contribution to the observed suppression of moderate p_T hadrons in $A + A$ data can be calculated,

thereby making it possible to isolate the contribution due to jet quenching.

In conclusion, calculations based on the HIJING model reveal quantitatively the important role of multiple minijet production in ultrarelativistic heavy ion collisions. We emphasized here two novel nuclear effects which influence strongly the absolute yield of moderate p_T hadrons, namely gluon shadowing and jet quenching. Both effects are of fundamental interest as they pertain to nuclear structure at the partonic scale and the energy loss mechanisms in dense matter. We showed that a systematic study of moderate p_T single inclusive hadron spectra in $p + p$, $p + A$, and $A + A$ collisions can be expected to provide enough information to determine the magnitude of each effect separately. The expected nuclear dependence of those spectra are large and should be readily measurable at RHIC.

- [*] X.-N. Wang and M. Gyulassy, Phys. Rev. Lett. **68**, 1480 (1992).
- [1] L. L. Frankfurt and M. I. Strikman, Phys. Rep. **160**, 235 (1988); F. E. Close, J. Qiu and R. G. Roberts, Phys. Rev. D **40**, 2820 (1989); A. H. Mueller Nucl. Phys. **B335**, 115 (1990).
- [2] M. Gyulassy and M. Plümer, Phys. Lett. **243B**, 432 (1990).
- [3] EM Collaboration, J. Ashman, *et al.*, Phys. Lett. **202B**, 603 (1988); M. Arneodo, *et al.*, Phys. Lett. **211B**, 493 (1988).
- [4] M. Gyulassy, M. Thoma and X. N. Wang, LBL preprint LBL-31003 (1991).

2.4. Minijet Contribution to the Background of Direct Photons

(L. K. Srivastava, B. Sinha, M. Gyulassy, X.-N. Wang [*])

Since minijets are so copious in heavy ion collisions, they must contribute to the background of the proposed signatures of a quark gluon plasma. These backgrounds must be carefully studied in order to recognize the new physics associated with QGP phase transition. In this paper we discuss the contamination of high p_T direct photons from decay photons such as $\pi^0 \rightarrow 2\gamma$. Direct photons produced by the QGP can be used to measure the initial temperature [1] as they interact only electromagnetically on their way out.

One of the aims of this study is to compare the yield of photons from an assumed equilibrated QGP to the yield of photons produced in the absence of equilibration, especially the electromagnetic decay of the final hadrons which could have relatively large p_T . The largest background is expected from the $\pi^0 \rightarrow 2\gamma$ decay. Decay photons must be efficiently subtracted out in order that the sought after dynamical photons are not "dimmed out" [2] in their glare. In this paper, we make a conservative estimate for the yield of decay photons using HIJING model [3] in which the minijet at moderate p_T remains far out of equilibrium. We expect this to overestimate the decay background. For the dynamical photons we consider on the other hand an optimistic hydrodynamic scenario in which the main source of dynamical photons is equilibrated QGP and hadronic matter.

For the initial conditions we use the multiplicity densities and initial temperatures as estimated by Heinz *et al* [4] as upper and lower limits in a $Pb + Pb$ RHIC energies (~ 200 AGeV as reproduced in Table 1. The HIJING results for these collisions are within the range of those estimates.

The basic processes leading to emission of dynamical photons from a QGP, are the Compton ($qg \rightarrow \gamma g$) and the annihilation processes ($q\bar{q} \rightarrow \gamma g$). We assume that the transition temperature $T_C = 150 \text{ MeV}$, the freeze-out temperature $T_F = 140 \text{ MeV}$. Considering only longitudinal expansion, the thermal rate for the emission of photons from the QGP phase due to these processes in a collision of two nuclei A and B integrated over the space-time history of the plasma, has been evaluated to give,

$$\frac{dN_{\gamma, QGP}}{d^2 p_T dy}(y \approx 0) = \frac{K}{p_T^4} F\left(\frac{p_T}{T_C}, \frac{p_T}{T_0}\right), \quad (1)$$

where $F(b, a) = \int_a^b dt e^{-t} t^{2.5}$, and

$$K = \alpha \alpha_s \log(2/\alpha_s) \left\{ \frac{(R_A + R_B)^2}{R_A R_B} \frac{c}{4a} \frac{dN}{dy_\pi} \right\}^2 \frac{4\sqrt{2}\pi}{\pi^4} \frac{1}{\pi R_A^2}. \quad (2)$$

Quantity	RHIC
$\sqrt{s}(\text{GeV}/A)$	200
α	0.0-0.2
dN/dy	670-2000
$\tau_0(\text{fm}/c)$	1
$T_0(\text{MeV})$	179-259
T_0/T_C	1.19-1.73
$\tau_0(\tau: 1/3T_0)(\text{fm}/c)$ (see text)	0.22-0.13
$T_0^\dagger(\text{MeV})$	292-504
T_0^\dagger/T_C	1.9-3.4

[†] Upper half adopted from Heinz et al [4]

Table 1: Multiplicity density and initial temperature[†] for $^{208}\text{Pb}+^{208}\text{Pb}$ system at RHIC energies.

For evaluating the contributions from the mixed phase, we make a simplifying assumption that the rate for emission of dynamical photons from quark matter is identical to the same from hadronic matter at $T = T_c$ consistent with detailed results of Kapusta et al [5]. The contribution from the quark-matter in the mixed phase is then

$$\frac{dN_{\gamma, QM}^{Mixed}}{d^2 p_T dy}(y \approx 0) = \frac{K(r-1)}{6p_T^4} \left(\frac{p_T}{T_C}\right)^{3.5} e^{-p_T/T_C}, \quad (3)$$

where $r = a_Q/a_H$ is the ratio of the number of the degrees of freedom in the QGP and the hadronic phases. Similarly, the contribution of the hadronic matter in the mixed phase is obtained as

$$\frac{dN_{\gamma, HM}^{Mixed}}{d^2 p_T dy}(y \approx 0) = \frac{Kr(r-1)}{6p_T^4} \left(\frac{p_T}{T_C}\right)^{3.5} e^{-p_T/T_C}. \quad (4)$$

Finally, the contribution of the hadronic phase to dynamical photons is given by

$$\frac{dN_{\gamma, Had. Pha.}}{d^2 p_T dy} (y \approx 0) = \frac{Kr^2}{p_T^4} F\left(\frac{p_T}{T_F}, \frac{p_T}{T_C}\right). \quad (5)$$

The sum of (1) and (3) is the contribution of the plasma and similarly the sum of (4) and (5) is the contribution of the hadronic matter. For the given initial condition with $T_0/T_C \approx 1.7$ we find that the number of photons from QGP phase becomes larger than the hadronic phase beyond $p_T \approx 2$ GeV/c. In this region, the plasma would out-shine the hadronic matter considerably if $T_0/T_C \approx 3$.

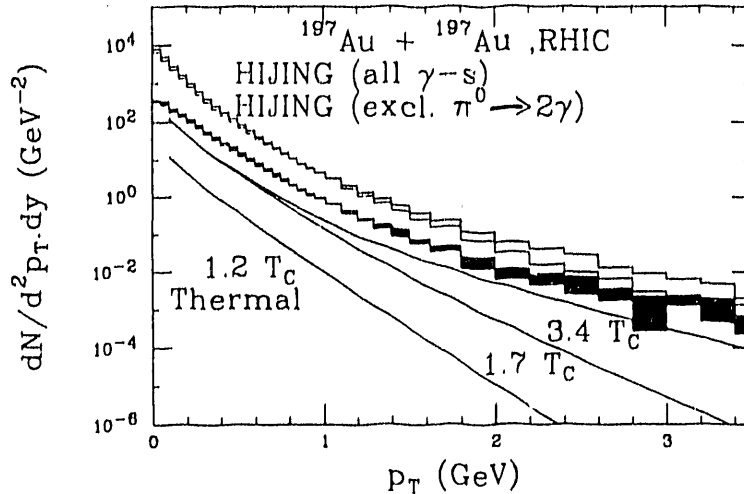


Fig. 1: Dynamical photon yields from the quark matter (solid lines) for different initial conditions compared to decay photons as estimated in the HIJING model. The dark shaded region corresponds to the yield of decay photons *excluding* the $\pi^0 \rightarrow 2\gamma$ decay. The lower and upper histograms (at higher p_T) for each case correspond to the cases with and without final state interactions in HIJING.

To study the background from electromagnetic decay of hadrons, We show in Fig. 1 the upper and lower limits of the rates for photons from the quark matter in a typical central collision of two gold-nuclei at RHIC energies for initial conditions given in Table 1, in a QGP scenario along with the predictions of photon production by HIJING. The HIJING estimates provide the the sum of all the photons, (upper histograms) and the ideal situation when all the photons originating from the decay $\pi^0 \rightarrow 2\gamma$ are excluded (lower histograms). The background could be decreased further if the photons from the decay of η mesons are also identified. We also show the uncertainties in HIJING due to final state interactions of among minijets. We see that within the uncertainties inherent these models the yield of dynamical photons from the quark-matter in the p_T region above 2 GeV/c is small relative to the the yield of decay photons unless the initial temperature is very high.

In summary, we have calculated the yield of dynamical photons from central collisions of ultra-relativistic nuclei at RHIC energies in a hydrodynamic model of QGP expansion and compared it the yield from electromagnetic decays in a model dominated by minijet production. We find that if $T_0 > 2T_C$ the dynamical photons from the equilibrated quark

matter dominate over the dynamical photons from the equilibrated hadronic matter for $p_T > 2\text{GeV}$. However, in this region the background of decay photons is at least an order of magnitude higher. If the abundant decay photons can be reliably subtracted, then the dynamical photons having $p_T > 2\text{ GeV}$ may indeed prove to be a useful thermometer of the initial conditions in the quark gluon plasma.

- [*] D. K. Srivastava, B. Sinha, M. Gyulassy, X.-N. Wang, Phys. Lett. **B276**, 285 (1992).
- [1] S. Raha and B. Sinha, Int. J. Mod. Phys. **A6**, 517 (1991), and references therein.
- [2] V. Ruuskanen, Proc. Quark Matter 91, to be published.
- [3] X.N.Wang and M. Gyulassy, Phys. Rev. D **44**, 3501 (1991); **45**, 844 (1992).
- [4] U. Heinz, P. Koch and B. Friman, Proceedings Large Hadron Collider Workshop, Aachen (1990), CERN-90-10, vol.II, p.1079.
- [5] J. Kapusta, P. Lichard and D. Seibert, University of Minnesota preprint (1991).

3. LATTICE GAUGE THEORY

3.1. *Deterministic Chaos in Non-Abelian Lattice Gauge Theory*

(B. Müller, A. Trayanov[†] [*])

Knowledge of the microscopic mechanisms responsible for the local equilibration of energy and momentum in central relativistic nuclear collisions is essential for our understanding of the quark-gluon plasma. The most commonly applied model assumes that the collision energy is first stored in coherent glue-field configurations (flux-tubes), which later break up by spontaneous creation of quark-antiquark pairs. However, it can be argued that energy-momentum equilibration could occur more rapidly via a cascade of perturbative gluon interactions with little contribution, initially, from quarks [1,2]. This might lead to the formation of an equilibrated system of gluons with higher initial temperature [3]. It is, therefore, of interest to investigate mechanisms of entropy production in non-abelian gauge theories in the absence of quarks. Whereas transport and equilibration processes have been extensively studied in the framework of perturbative quantum chromodynamics (QCD), rigorous non-perturbative studies of non-abelian gauge theories have been limited to systems at thermal equilibrium. We have undertaken a numerical study of real-time evolution in the classical, i.e. unquantized, version of the lattice gauge theory. The results of such an analysis should provide valuable insight into the dynamical properties of non-abelian gauge theories, in particular, at high excitation energies. The usefulness of investigations of the classical lattice gauge dynamics for highly excited states was first realized and employed in studies of baryon-number violating processes in the SU(2)-gauge-Higgs system at high temperature [4].

As explained below, we have found numerical evidence that the Hamiltonian classical dynamics of SU(2)-gauge theory (Yang-Mills theory) on a three-dimensional lattice is deterministically chaotic, and we have determined the rate of exponential divergence of adjacent gauge configurations. We note that classical Yang-Mills theory is known to be a non-integrable dynamical system [5,6]. Moreover, the presence of chaotic dynamics has been reported before in the context of radially symmetric solutions of classical SU(2)-gauge theory [7] but not for general solutions of Yang-Mills dynamics in three spatial dimensions.

Our study is based on the Hamiltonian formulation of lattice SU(2)-gauge theory [8,9], governed by the Hamiltonian

$$H = \frac{g^2}{a} \left\{ \sum_{\ell} \frac{1}{2} E_{\ell}^a E_{\ell}^a + \lambda \sum_p [1 - \cos(\frac{1}{2} B_p)] \right\}, \quad (1)$$

where g is the coupling constant, $\lambda = 4/g^4$, and a denotes the lattice spacing. The electric and magnetic fields are expressed in terms of the SU(2) link variables $U_{\ell} = \exp(-i\frac{1}{2}\tau^a A_{\ell}^a)$ as:

$$E_{\ell}^a = -i\frac{a}{g^2} \text{tr}[\tau^a \dot{U}_{\ell} U_{\ell}^{-1}], \quad \cos(\frac{1}{2} B_p) = \frac{1}{2} \text{tr} U_p. \quad (2)$$

U_p is the product of all four link variables on an elementary plaquette, and the dot denotes a time derivative. We numerically integrate the equations of motion resulting from the Hamiltonian (1) with a sufficiently small time-step to ensure conservation of energy and of

Gauss' law to at least six significant digits. In order to observe the exponential divergence of two trajectories $U_\ell(t), U'_\ell(t)$ in the space of gauge field configurations we introduce the following gauge-invariant metric:

$$D(U_\ell, U'_\ell) = \frac{1}{2N_p} \sum_p |\text{tr}U_p - \text{tr}U'_p|. \quad (3)$$

D is proportional to the absolute local difference in the magnetic energy of two different gauge fields. We note a peculiar property of this distance measure, which is a natural consequence of the topology of the compact $6N^3$ -dimensional space of gauge configurations on a N^3 lattice: For $N \gg 1$ almost all pairs of configurations have the same distance D . This property does not limit the usefulness of the metric (3) as measure of the divergence of infinitesimally separate field configurations, but it causes the saturation of D at large times observed in the calculations (see figures below).

Fig. 1 shows the evolution of $D(t)$ for initially neighboring gauge field configurations on a 20^3 lattice. We choose the reference configuration by randomly selecting link variables in such a way that the average energy per plaquette takes on the desired value. This procedure is controlled by a parameter δ which varies between 0 and 1. We then construct a neighboring configuration by perturbing each link element infinitesimally (for technical details, see [*]).

For values of δ of order unity the distance $D(t)$ starts to grow exponentially as $D(t) = D_0 \exp(ht)$ almost immediately (see Fig 1a). The growth rate h decreases with δ , and for $\delta \ll 1$ one observes an extended period during which the distance $D(t)$ between two adjacent field configurations performs more or less regular oscillations before exponential growth finally sets in (see Fig. 1b). For very small values of δ , corresponding to very low energy density of the gauge field configurations, the exponential growth pattern of $D(t)$ is modulated by low-frequency oscillations, which we attribute to the growing influence of non-leading Lyapunov exponents.

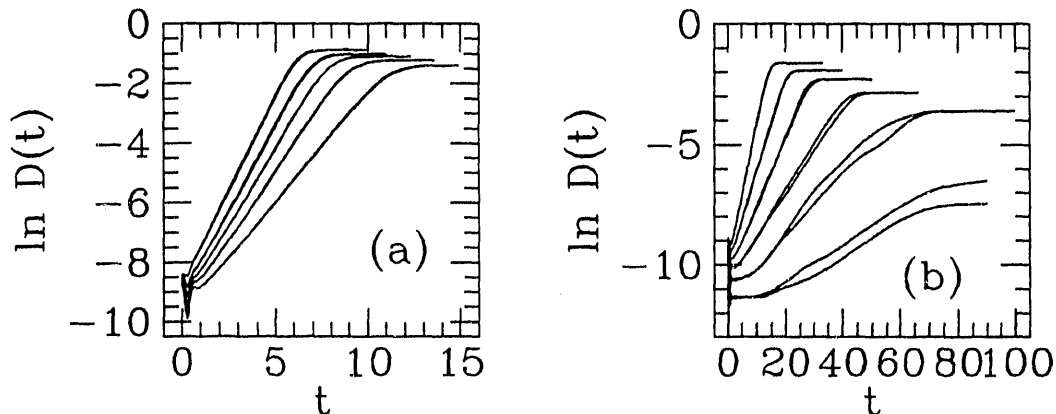


Fig. 1: Evolution of the distance $D(t)$ between neighboring random gauge field configurations for several average energies on a 20^3 lattice. The curves correspond, from top to bottom, to the parameters (a) $\delta = 1, 0.5, 0.45, 0.4, 0.35$; (b) $\delta =$

0.3, 0.25, 0.2, 0.15, 0.1, 0.05. For every value of δ two curves are shown, which are indistinguishable when $\delta > 0.2$.

Extensive studies have shown that the growth rate h is a universal function of the average energy per plaquette E , as shown in Fig. 2. For values $\delta > 0.15$, covering the physically relevant range of energy densities, the numerical determination of $h(E)$ from $D(t)$ is quite reliable, and the statistical and systematic errors are small. Fig. 2 shows that $h(E)$ is growing approximately linearly with energy. The dependence of h on the other relevant parameters, i.e. g and a , can be easily derived from the scaling properties of the lattice Yang-Mills Hamiltonian (1). One finds that the dimensionless product ha can only be a function of the combination $g^2 Ea$. Our numerical results show that this function is approximately linear:

$$ha \approx \frac{1}{6} g^2 Ea. \quad (4)$$

This scaling property has been verified numerically over a wide range of values for g and a . We note that h is independent of the lattice spacing a in the semiclassical limit, where g does not run with a .

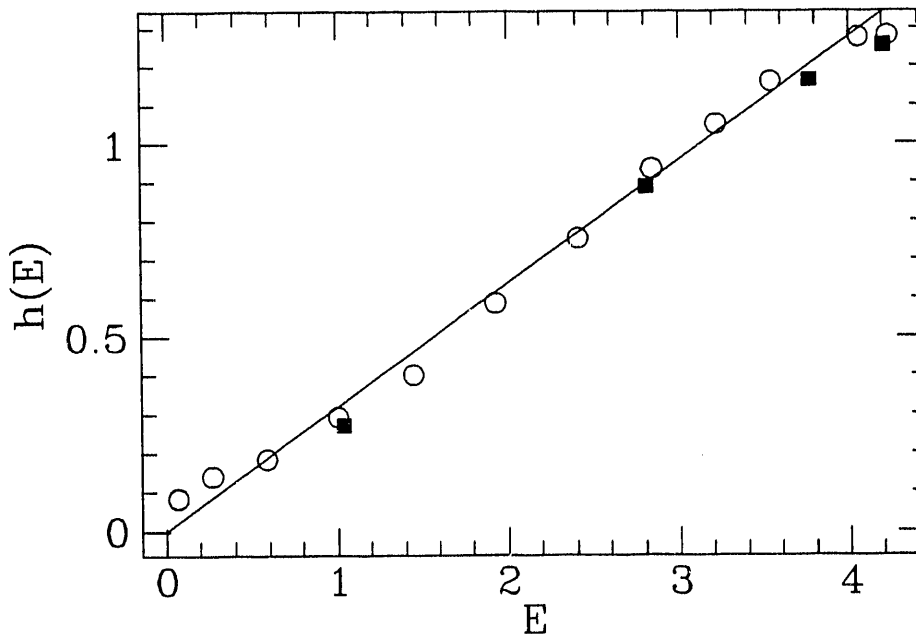


Fig. 2: Dependence of the exponential growth rate h on the average energy per plaquette E of the randomly chosen field configuration, for $a = 0.5$ and $4/g^4 = 1.1185$, and for lattice sizes $N = 20$ (open circles) and $N = 6$ (solid squares). The straight line through the origin is a least-squares fit.

We have also studied the dependence of $h(E)$ on the size of the lattice at fixed lattice spacing a over the range $N = 2 - 30$. While the fluctuations in $D(t)$ increase with diminishing lattice size, we have not observed within statistical errors a systematic dependence on N , for $\delta > 0.15$. The results obtained for $N = 6$ are shown in Fig. 2 as solid squares. For smaller values of δ we found that the exponential growth rate gradually decreases with

N , which may explain why the lowest two points in Fig. 2, obtained for $N = 20$, still lie above the straight line.

The universal exponential divergence of neighboring gauge field configurations implies that the entropy S of an ensemble of gauge fields grows linearly with time [10]: $S(t) = S_0 + \sum_i \lambda_i \theta(\lambda_i) t$, until the available microcanonical phase space is filled and the system is equilibrated. This implies that the characteristic entropy growth time (thermalization time) is given by

$$\tau_{\text{th}} = h^{-1} \approx 6/(g^2 E) \sim 6/(g^2 T), \quad (5)$$

if we identify the average energy per plaquette, E , with the physical temperature T (see [4]). This value is very close to the one derived for SU(3) gauge theory by Shuryak [3] on the basis of perturbative transport theory, suggesting that his result may be understood in the framework of semiclassical gauge field dynamics. Since our calculations were performed for the gauge group SU(2), our results are not quantitatively applicable to QCD, however, an estimate shows that $\tau_{\text{th}} \approx 0.5 \text{ fm}/c$ for $T = 300 \text{ MeV}$, if we insert the value of $g^2(T)$ obtained in thermal perturbation theory.

Chaoticity of the quantized Yang-Mills theory has been linked to the problem of color confinement [11]. If the ground state of Yang-Mills gauge theory would correspond to a chaotic distribution of field configurations, this fact would partially explain the difficulty of constructing a simple model of the QCD vacuum, because there exists no nontrivial field configuration, around which perturbative quantization can be performed in the standard way.

Acknowledgment: This work has been supported in part by a computing grant from the North Carolina Supercomputing Center.

† Also at: North Carolina Supercomputing Center, Research Triangle Park, NC 27709.

- [*] B. Müller and A. Trayanov, preprint DUKE-TH-92-32.
- [1] R. Hwa and K. Kajantie, Phys. Rev. Lett. **56**, 695 (1986).
- [2] K. Geiger and B. Müller, Nucl. Phys. **B369**, 600 (1992); B. Müller and X. N. Wang, Phys. Rev. Lett. **68**, 2437 (1992).
- [3] E. Shuryak, preprint SUNY-NTG-91-50.
- [4] J. Ambjørn, T. Askgaard, H. Porter, and M. E. Shaposhnikov, Nucl. Phys. **B 353**, 346 (1991); A. I. Bochkarev and Ph. de Forcrand, Phys. Rev. **D 44**, 519 (1991).
- [5] S. G. Matinyan, G. K. Savvidy, and N. G. Ter-Arutyunyan-Savvidy, Sov. Phys. JETP **53**, 421 (1981); JETP Lett. **34**, 591 (1981); B. V. Chirikov and D. L. Shepelyanskii, JETP Lett. **34**, 163 (1981); Sov. J. Nucl. Phys. **36**, 908 (1982).
- [6] G. K. Savvidy, Phys. Lett. **130 B**, 303 (1983); Nucl. Phys. **B 246**, 302 (1984).
- [7] S. G. Matinyan, E. B. Prokhorenko, and G. K. Savvidy, Nucl. Phys. **B 298**, 414 (1988); T. Kawabe and S. Ohta, Phys. Rev. **D 41**, 1983 (1990).
- [8] J. Kogut and L. Susskind, Phys. Rev. **D 11**, 395 (1975).
- [9] S. A. Chin, O. S. van Roosmalen, E. A. Umland and S. E. Koonin, Phys. Rev. **D 31**, 3201 (1985).
- [10] See e.g.: A. J. Lichtenberg and M. A. Leiberman, *Regular and Stochastic Motion* (Springer-Verlag, New York, 1983).
- [11] P. Olesen, Nucl. Phys. **B 200**, 381 (1982).

3.2. Thermalization in $SU(2)$ gauge theory

(A. Trayanov[†])

The $SU(2)$ Yang-Mills theory at finite temperatures has recently attracted an increasing attention with most of the studies mainly concentrated on the phase transition between the confinement and the free Coulomb phase [1,2]. The "standard" computational approach utilizes Monte Carlo simulations in 3+1 space and the periodicity in the Euclidian time is used to introduce temperature. Here we present a new, semiclassical approach to study the thermalization of the gauge fields in a Hamiltonian lattice gauge system coupled to thermal bath. The study is relevant to the equilibration time in quark-gluon plasma which may occur in neutron stars, heavy ion collisions, or the early universe.

The method we use is similar to the one used for the time evolution study of the gauge fields [3]. Three-dimensional space is discretized by a regular lattice, and the electric and magnetic gauge fields are defined on the links, connecting two neighboring vertices, and on the elementary plaquettes, forming the shortest closed path around a link, respectively. They are expressed in terms of $SU(2)$ variables:

$$U_\ell = \exp(-i\frac{1}{2}\tau^a A_\ell^a), \quad (1)$$

and

$$E_\ell^a = -i\frac{a}{g^2}\text{tr}[\tau^a \dot{U}_\ell U_\ell^{-1}], \quad \cos(\frac{1}{2}B_p) = \frac{1}{2}\text{tr}U_p. \quad (2)$$

Here U_p is the product of all four link variables on an elementary plaquette, and the dot denotes a time derivative.

The Hamiltonian of such system is

$$H = \frac{g^2}{a} \left\{ \sum_\ell \frac{1}{2} E_\ell^a E_\ell^a + \lambda \sum_p [1 - \cos(\frac{1}{2}B_p)] \right\}, \quad (1)$$

where g is the gauge coupling ($\lambda = 4/g^4$), and a is the lattice spacing.

To thermalize the system one has to couple it to a thermal bath. This will correspond to a physical system exchanging energy with gluons. The gluons can, in principle, emit or absorb both electric and magnetic energy. It is not difficult to implement each of these energy exchanges. For example, one can put or subtract electric energy simply by randomly generating a new set of time derivatives of the link variables, \dot{U}_ℓ , and accept or reject the replacement depending on the total energy change according to Boltzmann thermal distribution. The magnetic energy exchange, in turn, can be simulated by the so-called thermal bath method [4]. According to it, a new link variable, U_ℓ , is chosen in such a way, that the energy of the four plaquettes, which have the common link, is again picked up from the thermal distribution. The problem is reduced to generating points randomly on the surface of four-dimensional sphere with an exponential weight in a_0 direction.

The practical implementation of the thermalization requires, however, a different approach. The reason for this is that in each of the two mentioned exchange mechanisms the gluons can change the color charge at a given lattice site, which violates the Gauss law. To

avoid this, we modified the thermal bath method. The new link variable is chosen again with exponential weight in a_0 direction. The position of the new point on the surface of the 4D sphere in the other two directions is not chosen randomly, as in the original method [4], but in such a way that the new fields obey the Gauss law. This scheme provides thermalization of the magnetic part of the energy. Furthermore, the SU(2) lattice gauge system is chaotic [5], and therefore, ergodic. We utilize this fact and let the gauge dynamics distribute the energy over all degrees of freedom. At randomly chosen intervals the system is in thermal contact with "magnetic" bath, followed by periods of Hamiltonian determined evolution, during which the electric part of the energy is also thermalized.

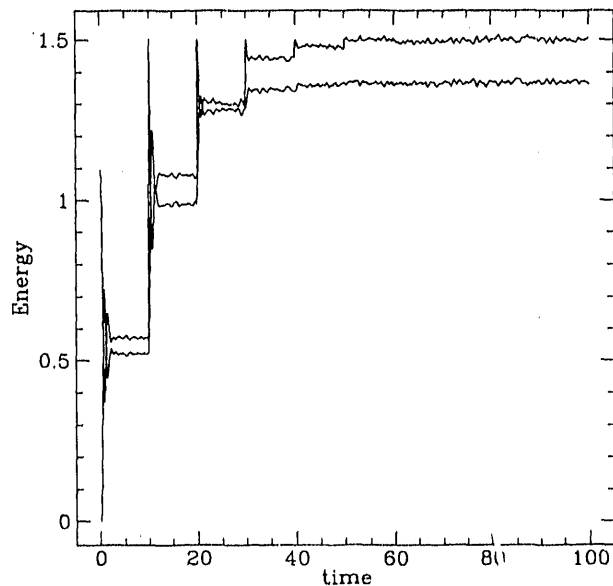


Fig. 1. Time evolution of electric and magnetic energies during thermalization. $T = 1.0$, $g^2 = 2$.

Figure 1 shows a typical behavior of electric and magnetic energies during the thermalization. During the evolution periods (no contact with the thermal bath) one can see the redistribution of the energy. After both energies reach a saturated region we plotted the distribution of the electric energy over all degrees of freedom. The histogram is shown on Figure 2. The linear behavior of the plot as well as the slope suggest that the energy is equipartitioned between all the degrees of freedom.

† Also at: North Carolina Supercomputing Center, Research Triangle Park, NC 27709.

- [1] L. D. McLerran and B. Svetitsky, *Phys. Lett.* **98B**, 195, (1981).
- [2] J. Kuto, J. Polónyi and K. Szlachányi, *Phys. Lett.* **98B**, 195, (1981).
- [3] A. Trayanov and B. Müller, preprint DUKE-TH-91-17, to appear in: *Computational Quantum Physics*, edited by A. S. Umar et al. (AIP, New York, 1992).
- [4] M. Creutz, *Quarks, gluons and lattices*, Chap. 13 (Cambridge University Press, Cambridge 1983).
- [5] B. Müller and A. Trayanov, preprint DUKE-TH-92-32, submitted to *Phys. Rev. Lett.*

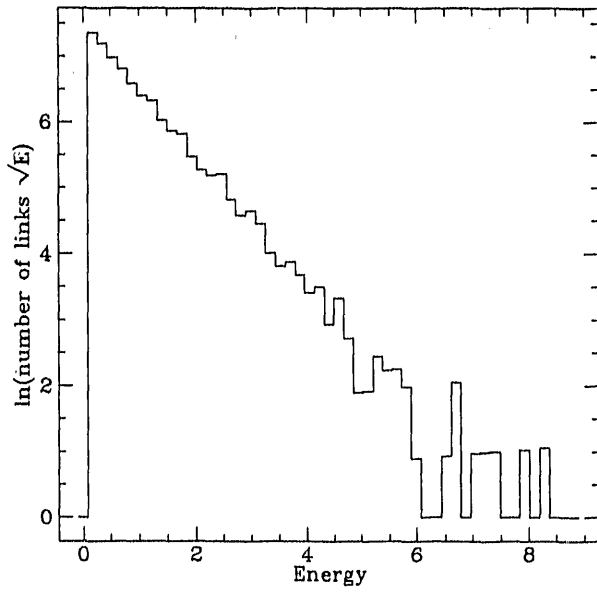


Fig. 2. Distribution of electric energy at $t = 100$.

4. HADRONIC MATTER AND OTHER STUDIES

4.1. Nuclear Medium Effect on Kaon Dispersion Relation

(C.Gong [*])

For years enhancement of strangeness production has been studied as a possible signature of formation of quark-gluon plasma [1]. The basic argument is that the formation of quark-gluon plasma reduces the threshold of strangeness production. But it is also argued that enhancement of strange hadron production can be explained in a hadronic scenario [2]. So in order to unambiguously identify it, we need to have a better understanding of the behavior of strange hadrons in hot hadronic gas. In this work, we have studied the modification of the kaon dispersion relation due to the surrounding hadrons in a thermalized hadronic system with a model independent method [3].

If the system is not too dense, we can make an approximation to take into account only two body interactions. Then we have a simple representation for induced self-energy $\Sigma(p)$ of a hadron in a gas of hadrons:

$$\Sigma(p) = - \int \frac{d^3 k}{(2\pi)^3} \frac{8\pi f(0)}{2\omega \sqrt{s}} n(k), \quad (1)$$

where $f(0)$ is the forward scattering amplitude of the studied hadron with an environmental hadron, $n(k)$ is thermal distribution of the environmental hadron and ω, k are its energy and momentum, respectively. With $\Sigma(p)$, we define a potential for the hadron in hadronic gas as follows:

$$V(p) \equiv E(p) - E_0(p), \quad (2)$$

where

$$E(p) = (p^2 + m^2 + \Sigma(p))^{1/2}, \quad E_0(p) = (p^2 + m^2)^{1/2}. \quad (3)$$

We use this method to study the modification of the kaon dispersion relation in hot hadronic gas. We calculate contributions from pions and nucleons which are two most abundant particles in the gas. For the pion contribution we use the resonance approximation, where we take K^* as the dominant channel in the $K - \pi$ scattering and we use a Breit-Wigner formula to obtain the forward scattering amplitude. For the nucleon contribution we use experimental data for the $K - N$ forward scattering amplitude [5]. The fit for real part of $f(0)$ is obtained as a function of kaon incident momentum p . The sign of $f(0)$ is negative for K^+N scattering and positive in the K^-N channel. Here we only calculate the real part of the potential.

Adding the pion and nucleon contributions together for both K^+ and K^- , we notice two interesting things. Firstly, since the dominant contribution comes from nucleons, the potential increases fast with baryon density n . Secondly, due to the different behavior of K^+N and K^-N scattering, the signs of the nucleon contributions to K^+ and K^- are different. So the net potential also has a different sign for K^+ and K^- . This implies that K^+ and K^- will have quite different behavior in high baryon density gas.

Here we study an important consequence which is closely related to the difference of K^+ and K^- behaviors in nuclear matter. This is the change of K^+ and K^- abundance

ratio in a hadronic gas. This ratio has been calculated without taking into account of the potential effect, where it grows rapidly with baryon density [6]. It is suggested that by measuring this ratio, one may determine the baryon chemical potential μ_b [1]. Considering the effective in-medium potential we calculated, we find a different behavior. The results are compared in Fig. 1, where the ratio is shown as a function of baryon density and baryon chemical potential. Our result shows that the ratio grows much slower at low baryon density, moreover it stops growing at some density and has a tendency to decrease at high density. The ratio is never very large and is between 2 to 3. The same number from AGS is around 4-5. Of course we should not trust the result at high density too much because of the second assumption made above. But our result says that it will be difficult to deduce μ_b from this ratio.

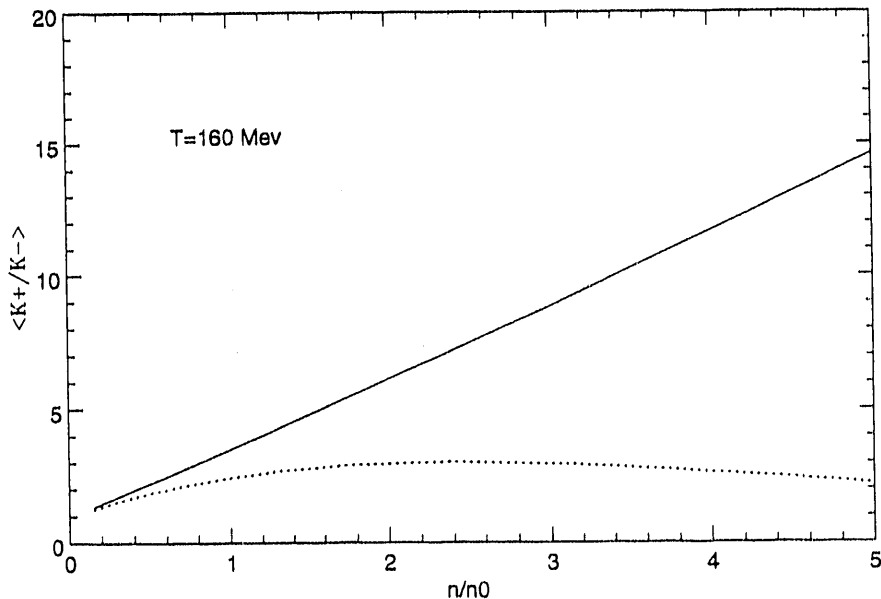


Fig. 1: Density ratio of K^+ and K^- as a function of baryon density.

- [*] C. Gong, preprint DUKE-TH-92-31, J. Phys. **G**, in print.
- [1] P. Koch, B. Müller, J. Rafelski, Phys.Rep. **142**, 169 (1986).
- [2] C.M. Ko et al, Phys.Rev.Lett. **66**, 2577 (1991).
- [3] E.V. Shuryak, Nucl. Phys. **A533**, 761 (1991).
- [4] E.V. Shuryak, V.Thorsson, SUNY preprint SUNY-NTG-91-30.
- [5] B.R. Martin, Nucl. Phys. **B94**, 413 (1975); O.V. Dumbrajs, Nucl. Phys. **B26**, 497 (1971); E.A. Veit, Phys. Rev. **D31**, 1037 (1985); P.J. Fink, Phys. Rev. **C41**, 2720 (1990).
- [6] P. Koch, J. Rafelski, W. Greiner, Phys. Lett. **123B**, 151 (1983).

4.2. *Non-equilibrium Statistical Field Theory* (J. Rau)

A central collision of ultrarelativistic heavy ions creates a region of extremely high energy density. This region is characterized by very strong (chromo-)electric and magnetic fields; they subsequently decay into a large number of particles. The decay process exhibits

an important feature: Energy is *irreversibly* transferred from one type of fields (i.e., the gauge fields) to another, namely the matter fields. In particular, the coherence of the initial state is lost entirely (“decoherence” [1]). So far no general mathematical framework exists for the description of such irreversible processes involving relativistic elementary particle reactions. Indeed, it is unclear how exactly and at which rate entropy is produced during these processes.

Unitary time evolution leaves the entropy constant; to explain its increase, other mechanisms must be taken into consideration: Either, the forces acting on the system are not completely known, and thus the interaction has to be described by a stochastic Hamiltonian. Or, only a certain set of observables is actually measured in the experiment (e.g. only single particle observables, but no correlations), and for the sake of simplifying calculations, irrelevant information not referring to the preferred set of observables is voluntarily discarded [2].

In the latter case, the ‘true’ statistical operator can be replaced by its “relevant part”; the relevant part is determined at all times using the maximum entropy principle. Its time evolution is described by the Robertson equation [3]:

$$\dot{\rho}_t^{\text{rel}} = -iP_t L \rho_t^{\text{rel}} - \int_{t_0}^t dt' P_t L T_{tt'} Q_{t'} L \rho_{t'}^{\text{rel}} \quad (1)$$

Here L is the Liouville operator, P and Q are orthogonal projection operators in Liouville space, and T is a time evolution operator in Liouville space. The Robertson equation differs from the v. Neumann equation mainly by the integral (‘memory’) term. It leads to a system of non-linear equations for the expectation values of the preferred observables. To solve these equations, suitable approximations (e.g. perturbation theory) or numerical methods have to be employed.

- [1] W.H. Zurek, Phys. Rev. D **24**, 1516 (1981); Phys. Rev. D **26**, 1862 (1982).
- [2] E.T. Jaynes, Phys. Rev. **106**, 620 (1957); Phys. Rev. **103**, 171 (1957); Am. J. Phys. **33**, 391 (1965).
- [3] E. Fick and G. Sauermaun, *The Quantum Statistics of Dynamic Processes*, (Berlin, Heidelberg: Springer 1990).

4.3. Applying Neural Networks to Resonance Search

(Dena McCown, J. Rau)

It is the aim of many experiments in high energy physics to discover and investigate the properties of rare particles, but it is often very difficult to discover their signature against the background. Recently it has been suggested that neural networks may be used very effectively to suppress the background and thus enhance the relative strength of the signal [1,2,3]. The objective of this project was to investigate whether or not neural networks can perform an unbiased data analysis, specifically whether or not the network trained better in polar or Cartesian coordinates when learning a circular pattern.

The network used has two inputs, one hidden layer, and one output. It was trained using error back propagation [4]. Initially, several simple data sets were tested on the network. Half of the data was coded with a 1 for signal, and the other half was coded

with a 0 for background. Number of hidden layers, units per layer, and points fed to the network were all variables. The network performed best for all data sets with 2 hidden layers (maximum allowed), 15 units per layer, and 200 points.

The final test was a double pattern with a rectangle (0) and a ring (1). The input pattern is denoted as *Text* in the Figure. The network was trained on this configuration both in Cartesian and polar coordinates and with the rectangle and ring overlapping and the rectangle completely inside of the ring. The results showed that the network learns this pattern much better when trained in polar coordinates and when the rectangle is completely inside of the ring. A graph of the final output illustrates the difference. In conclusion, it is very important to have a suitable pre-processor for the data before feeding it to the network.

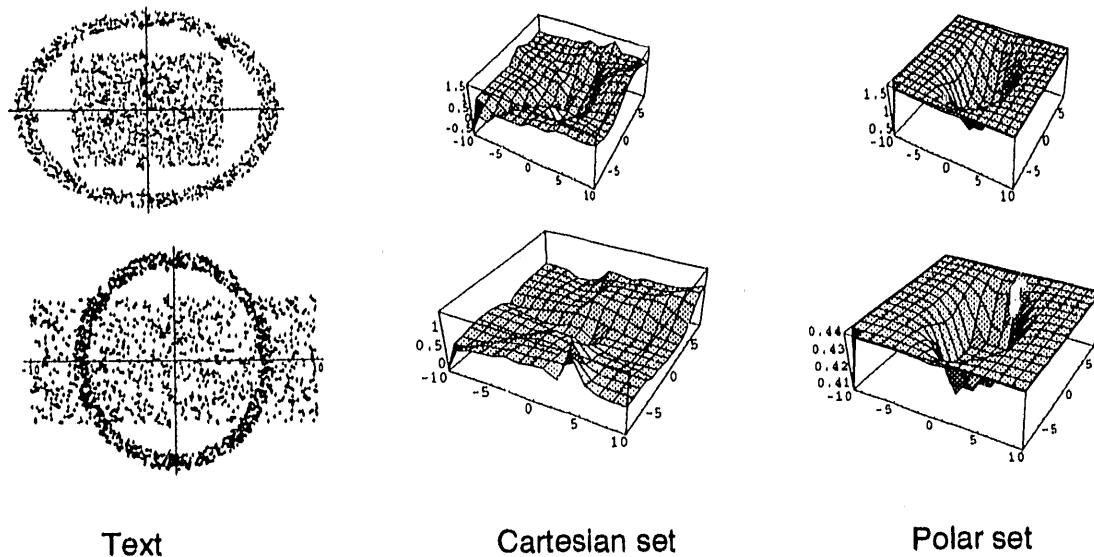


Fig. 1: Configurations.

- [1] B. Denby, *Comp. Phys. Comm.* **49**, 429 (1988).
- [2] B. Humpert, *Comp. Phys. Comm.* **56**, 299 (1990).
- [3] T. Alexopoulos, Ph.D. thesis, University of Wisconsin – Madison 1991 (unpublished).
- [4] see e.g.: B. Müller and J. Reinhardt, *Neural Networks – an Introduction*, Springer, Heidelberg, 1990; J. Hertz, A. Krogh, and R.G. Palmer, *Introduction to the Theory of Neural Computation*. Addison-Wesley, Redwood City, 1991.

4.4. The formation of $\pi^- \pi^+$ -atoms in relativistic heavy ion collisions (E. van Doorn)

Recent heavy-ion collision experiments have yielded data on the production of composite particles from a region of very dense and highly excited hadronic matter. The formation of composite particles is a two-step process. First, mesons and baryons are formed when quarks and gluons coalesce into colorless objects. The second step is the coalescence of two or more simple hadrons. If composite, weakly bound particles, like a $\pi^- \pi^+$ -atom, were formed directly from the QGP, collisions with other particles would break them up immediately as the binding-energy is small compared to the available center of mass energy.

Dover et al [1] developed a relativistic coalescence model that only considers the second step (the coalescence process between produced hadrons) to estimate the production rate for light (anti)nuclei, the H-dibaryon and the penta-quark in relativistic heavy ion collisions at CERN SPS and Brookhaven AGS accelerators. This model is based on the coalescence formula:

$$N_C = \int f(x_i; p_i) C(x_i; p_i) \prod_{i=1}^2 \left(\frac{2\theta(p_i^0) \delta(p_i^2 - m_i^2) d^4 p_i}{(2\pi\hbar)^3} p_i^\mu d\sigma_i^\mu \right), \quad (1)$$

where N_C is the number of composite particles formed and $f(x_1; x_2; p_1; p_2)$ is the two-particle distribution function in phase space, which depends on the space-time and the energy-momentum coordinates of the two coalescing particles. The Lorentz scalar function C is called the "coalescence factor". It depends on Lorentz invariant combinations of the relative coordinates between the two coalescing particles and parametrizes the overlap integral between the particle wavefunctions as it would occur in an underlying quantum mechanical treatment. Gaussian parametrization (consistent with using h.o. wavefunctions) is used for the hadrons and the cluster.

The single particle distributions used feature a Gaussian rapidity distribution and have an exponential dependence on the transverse mass, m_\perp , with a slope parameter T in the region of a couple of hundred MeV . The quantity actually calculated is the *coalescence probability* $C^{(1)}$, defined by:

$$\frac{dN_C}{dY} = C^{(1)} \frac{dN_1}{dy_1} \frac{dN_2}{dy_2}, \quad (2)$$

where $\frac{dN_1}{dy_1}$, $\frac{dN_2}{dy_2}$ are the parent particle rapidity distributions.

I applied this model to calculate the coalescence probability for the $\pi^- \pi^+$ -atoms, using experimentally obtained pion spectra [2]. The coalescence probabilities turned out surprisingly large (of order 10^{-5}), amounting to the formation of one $\pi^- \pi^+$ -atom every two hundred collisions. The lifetime of the $\pi^- \pi^+$ -atom, $\sim 10^{-16}$ s allows it to travel outside the "fire-ball", where its decay into two neutral pions (four photons) might be observed. A comprehensive study of the formation probabilities of other meson-meson atoms, and of the chances for their observation, is in progress.

[1] C.B. Dover, U. Heinz, E. Schnedermann and J. Zimányi, Phys. Rev. C44, 1636 (1991).

[2] T. Abbott et al. (E-802 Collaboration), Phys. Rev. Lett. 64, 847 (1990).

4.5. Finite Volume Effects on Gluon Plasma

(C. Villarreal)

When a head-on heavy ion collision occurs, it is expected that hot and compressed nuclear matter is confined in a small region of space. In Au-Au collision, this region should have a radius about 6.5 fm and a depth of 1 fm. In such circumstances, finite volume effects may become relevant when studying the properties of the quark gluon plasma (QGP). The QGP is generally studied in the infinite volume thermodynamic approximation, where the single particle energy levels may be replaced by a continuous distribution. However,

this approximation may not be necessarily true in the region of formation of the QGP. In particular, it may be shown that the thermodynamic properties of a gas are no longer isotropic and that the equation of state should be written as $e = p_x + p_y + p_z$, where e is the energy density of the gas and p_k is the pressure in the k direction.

The Casimir effect has been studied for a baryon-free QGP confined in an infinite slab region [1]. It was found that the energy and entropy densities at the transition temperature are 2 or 3 times as large as those of unconfined QGP when the width of the slab is about 1 fm. However, the Casimir energy is strongly dependent on the geometry of the system. Thus, it is natural to inquire how these results are modified when considering a gas confined into a finite region of space. For such purpose, the energy-momentum spectrum of vacuum fluctuations of a spin-1 field satisfying bag boundary conditions in a rectangular cavity was calculated using a finite temperature Green function formalism [2]. This method generalizes previous zero-temperature calculations [3]. The frequency integrated renormalized expression of the T_{oo} component is:

$$\begin{aligned}
 T_{oo} = & \frac{\pi^2}{15} T^4 - \frac{\pi}{24} \frac{(a+b+c)}{V} T^2 \\
 & - \frac{\pi}{2} T^3 \sum_{lmn=-\infty}^{\infty} \frac{\cosh[2\pi T U_{lmn}]}{U_{lmn} \sinh^3[2\pi T U_{lmn}]} \\
 & + \frac{\pi}{4V} T^2 \sum_{l=-\infty}^{\infty} \left[\frac{a}{\sinh^2[2\pi a T l]} + \frac{b}{\sinh^2[2\pi b T l]} + \frac{c}{\sinh^2[2\pi c T l]} \right], \quad (1)
 \end{aligned}$$

where $U_{lmn} = \sqrt{(al)^2 + (bm)^2 + (cn)^2}$, T the temperature, V the volume, and a, b, c , the lengths of the cavity. The ratio R of confined energy density and free energy has been evaluated as a function of the width z of a region with typical dimensions $a = b = 13$ fm, and at temperature of 150 Mev. The result is sketched in Fig.1.

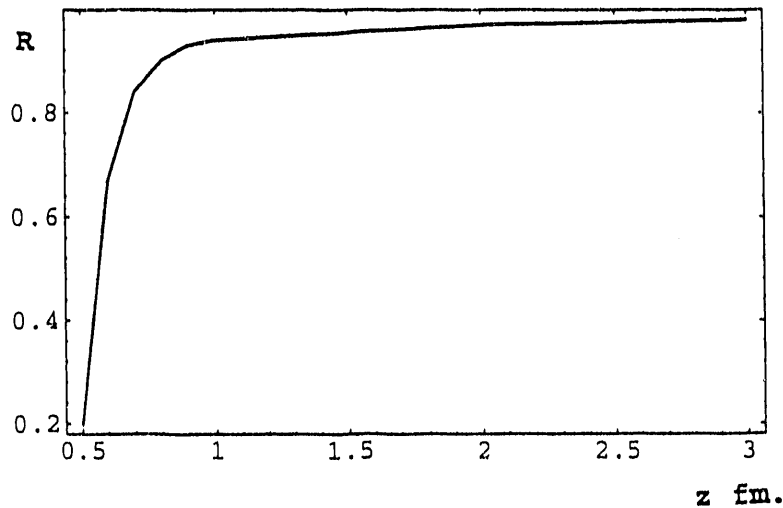


Fig. 1: Energy ratio as function of the width z of the cavity.

In these preliminary calculation, it turns out that finite size effects are appreciable when the confining region has a width of the order of 0.5 fm. For lengths greater than

1 fm., these effects seem to be irrelevant. Of course, more detailed calculations must be performed. In particular, fermion contributions which, up to now, have not been successfully calculated for this geometry must be estimated, as well as generalizations to more realistic geometries. The detailed thermodynamic behavior of this model is in progress.

- [1] K. Saito, Z .Phys. C **50**, 69 (1991).
- [2] C. Villarreal, to be published.
- [3] S. Hacyan, R. Jáuregui, and C. Villarreal, Preprint IFUNAM (1991).

5. STRONG ELECTROMAGNETIC FIELDS

5.1. *Exact Dirac Propagator in a Magnetic "Sheet"*

(B. Müller, A.J. Schramm, S. Schramm [*])

There are not many electromagnetic field configurations for which the exact analytical form of the Dirac propagator is known. The solution reported here was motivated by the observation that in peripheral collisions of charged particles at high energy the electromagnetic field strengths become very large at the point of closest approach. For projectiles of like charge the electric field between passing particles is strongly suppressed, whereas the magnetic fields are additive.

In a peripheral collision of two identical nuclei in the c.m. frame at very high energy the electromagnetic fields are extremely Lorentz contracted in the beam direction. Since this extension is small compared to the typical length scale of particles moving in this field, we describe the magnetic field by a δ -function along z , i.e.

$$\vec{B} = \xi \delta(z) \vec{e}_x \quad (1)$$

which approximates the maximum in the \vec{B} -field evolution during the collision process at the point of closest approach of the two ions, $z = 0$. Eq. (1) describes a "magnetic sheet" perpendicular to the beam axis. The constant ξ can be determined by demanding that the line integral of the magnetic field along the z -axis should give the same value for the idealized field (1) as for the realistic field configuration produced by the moving charges:

$$\xi = \left| \int d\vec{n} \times \vec{B} \right| = \frac{1}{4\pi} \int_{-\infty}^{\infty} dz \frac{2Ze\gamma}{(\gamma z)^2 + \frac{1}{4}b^2} = \frac{Ze}{b} \quad (2)$$

As a result, the Lorentz factor γ does not appear in Eq. (1).

We are interested in determining the Dirac propagator $S(x, x')$, satisfying the defining relation

$$(i\partial + qA_{\text{ext}} - m)S(x, x') = 0 \quad (3)$$

It is convenient to introduce the iterated propagator $G(x, x')$ defined as

$$S(x, x') = (i\partial + qA_{\text{ext}} + m)G(x, x'), \quad (4)$$

which satisfies a quadratic equation of motion:

$$\left[(i\partial + qA_{\text{ext}})^2 - m^2 - \frac{q}{2}\sigma_{\mu\nu}F^{\mu\nu} \right] G(x, x') = \delta^{(4)}(x - x') \quad (5)$$

The vector potential corresponding to the magnetic field configuration (1) can be taken as $A_y = -\xi\Theta(-z)$, $A_x = A_z = 0$.

The Fourier transformation of $G(x, x')$ in the x , y , and t coordinates yields a one-dimensional differential equation in z :

$$\left[\frac{d^2}{dz^2} + E^2 - m_{\perp}^2 - q\xi(q\xi - 2k_y)\Theta(-z) - q\xi\Sigma_x\delta(z) \right] G(z, z') = \delta(z - z'), \quad (6)$$

where $\Sigma_x = \sigma_{23}$ and $G(z, z') = G(E, k_x, k_y; z, z')$ is the propagator in momentum space in all directions except along the beam axis, where we keep the coordinate space representation. The transverse mass m_\perp is defined as $m_\perp^2 = m^2 + k_x^2 + k_y^2$. Since the differential operator has constant coefficients in the regions $z > 0$ and $z < 0$, the solution to eq. (6) can be found by matching the free Green functions $G_0(z, z')$ at the boundary $z = 0$.

These boundary conditions are even more obvious if we make a Wick rotation, replacing E by $(-iE)$. We will denote the Euclidean propagators as \tilde{G} . The resulting Green function reads

$$\tilde{G}(z, z'; s) = -\frac{1}{2k_+} \left[e^{-k_+(z-z')} + \frac{k_+ - k_- - sq\xi}{k_- + k_+ + sq\xi} e^{-k_+(z+z')} \right] \quad \text{for } (z > z'), \quad (7a)$$

$$\tilde{G}(z, z'; s) = -\frac{1}{2k_+} \left[e^{k_+(z-z')} + \frac{k_+ - k_- - sq\xi}{k_- + k_+ + sq\xi} e^{-k_+(z+z')} \right] \quad \text{for } (0 < z < z'), \quad (7b)$$

$$\tilde{G}(z, z'; s) = -\frac{1}{k_+ + k_- + sq\xi} e^{(k_- z - k_+ z')} \quad \text{for } (z < 0), \quad (7c)$$

where k_\pm are given by

$$k_+^2 = E^2 + m^2 + k_x^2 + k_y^2, \quad (8a)$$

$$k_-^2 = E^2 + m^2 + k_x^2 + k_y^2 - 2q\xi k_y + q^2 \xi^2. \quad (8)$$

This result may be inserted in Eq. (4) to obtain the Dirac propagator; we refrain from recording the result explicitly. An application of our result to the problem of possible W-boson condensation in collisions of charged particles at ultrahigh energies is discussed below in a separate section.

[*] S. Schramm, B. Müller, and A.J. Schramm, Phys. Lett. **164B**, 28 (1992).

5.2. W Boson Condensation in p-p Collisions?

(B. Müller, A.J. Schramm, S. Schramm [*])

Recently, the possibility of an intermediate W-boson condensate during a high energy proton-proton collision was discussed [1]. The key idea was that if two quarks with the same sign of electric charge come very close together (on the order of $r \sim 1/m_W$ where m_W is the mass of the W boson), the magnetic field between them is strong enough to generate an instability of the W-vacuum. The spectrum of a spin-1 particle with mass m and charge q in a homogeneous magnetic field pointing into the x direction is given by [2]:

$$E^2 = (2n + 1)qB - 2qBS_x + m_W^2 + p_x^2 \quad (1)$$

with non-negative integer n . $S_x = 0, \pm 1$ is the spin projection onto the x -axis. In the case of W-bosons one can see that a vacuum instability, $E < 0$, occurs for $S_x = 1$ if $eB > m_W^2$. At an impact parameter $b \sim 2/m_W$ for a collision of two up quarks one obtains a critical value of $\gamma \geq \frac{3}{4\alpha} \sim 100$, which is easily accessible. However, this estimate is only valid for a constant homogeneous magnetic field.

In an ultrarelativistic collision of two charged particles the electromagnetic fields are extremely Lorentz contracted in the beam direction. Since their extension is small compared to the typical transverse length scale we describe the magnetic field by a δ -function along z , i.e. $\vec{B} = \xi\delta(z)\vec{e}_z$ with $\xi = Ze/b$, as discussed in Section 5.1. (see ref. [3]). This configuration describes a "magnetic sheet" perpendicular to the beam axis. We neglect the fall-off of the field in transverse direction; this should be an acceptable approximation as long as the transverse momenta associated with a particular process are not below m_W .

The equation of motion of a W^+ boson in an external electromagnetic field $F_{\mu\nu} = \partial_\mu A_\nu - \partial_\nu A_\mu$ obeys the differential equation [4]:

$$\left\{ \left[(i\partial + eA)^2 - m_W^2 \right] g_{\mu\nu} - 2ieF_{\mu\nu} \right\} W^\nu(x) = 0 \quad . \quad (2)$$

where non-abelian self-coupling terms of the W field have been omitted. The fields W_y and W_z are coupled through the magnetic field $B_x \equiv F_{23}$. The diagonalization of the coupled equations yields

$$\left\{ \left[(i\partial + eA)^2 - m_W^2 \right] \pm 2eB_x \right\} W_s(x) = 0 \quad . \quad (3)$$

where W_s are the W fields which are polarized parallel ($s = +1$) and antiparallel ($s = -1$) with respect to the x -axis. The resulting equation for the W-boson field:

$$\left[-\partial^2 - m_W^2 - \Theta(-z)e\xi(e\xi + 2i\partial_y) - 2se\xi\delta(z) \right] W_s(x) = 0 \quad (4)$$

shows that the Green function of the W_\pm field satisfies the same differential equation as the iterated fermion propagator $G(x, x')$ defined in [3]. We need only make the replacement $q\Sigma_x \rightarrow 2es$, where the values of s and the eigenvalues of Σ_x are both given by ± 1 . The factor of 2 indicates the larger spin of the W - boson as compared to the spin- $\frac{1}{2}$ fermions. Hence the exact Green function of the W_\pm field in the "magnetic sheet" field is given by the same Green function derived in Section 5.1.

One can find bound states of the vector boson by investigating the pole structure of Eq. (5.1.7) which gives the spectrum of the particles in the magnetic sheet. Apart from the free particle pole for $k_+ = 0$, it exhibits poles for $k_+ + k_- + \kappa e\xi = 0$, with $\kappa = 1$ for fermions and $\kappa = 2$ in the case of vector bosons. Solving for E and rotating to Minkowski space one obtains the pole

$$E^2 = m^2 + k_x^2 + k_y^2 - \frac{1}{16} (2k_y + 3e\xi)^2 \quad . \quad (5)$$

For given field strength ξ the lowest energy is obtained for $k_y = e\xi/2$ and $k_x = 0$. Inserting these values into (5) one gets

$$E^2 \geq m^2 - \frac{3}{4} (e\xi)^2 \quad . \quad (6)$$

From Eq. (6) follows that W boson condensation sets in for field strengths $e\xi \geq \frac{4}{3} m_W$. With $\xi = 2e/3b$ this translates into a maximum value of the impact parameter for the onset of W condensation

$$b \leq \frac{2\pi\alpha}{m_W} \sim 0.045 m_W^{-1} \quad . \quad (7)$$

In these calculations we assumed an infinite extension of the magnetic field in the $x - y$ plane. This assumption is only warranted as long as the impact parameter b of the two scattering particles is much larger than the size of the Landau orbit in the magnetic field, or the inverse momenta, k_x^{-1} , k_y^{-1} , associated with the motion of the particle transverse to the beam direction. The result (7) severely violates this condition. The localisation of a state within the limit (18) requires an additional kinetic energy contribution of the order of $20 m_W$, which by far exceeds the attractive interaction with the magnetic field. Note that this argument is independent of the beam energy. Therefore the proposed process of W-boson condensation in high-energy p-p collisions does not work.

- [*] S. Schramm, B. Müller, and A.J. Schramm, Phys. Lett. **B277**, 512 (1992).
- [1] J. Ambjørn and P. Olesen, Phys. Lett. **B257**, 201 (1991).
- [2] V.V. Skalozub, Sov. J. Nucl. Phys. **41**, 1044 (1985).
- [3] S. Schramm, B. Müller, and A.J. Schramm, Phys. Lett. **164B**, 28 (1992).
- [4] J. Ambjørn, N.K. Nielsen, and P. Olesen, Nucl. Phys. **B310**, 625 (1988).

5.3. Quark-Antiquark Condensates in Strong Magnetic Fields

(B. Müller, A.J. Schramm, S. Schramm [*])

There is evidence that the vacuum of Quantum Chromodynamics (QCD) contains a condensate of quark-antiquark pairs and breaks chiral symmetry. Inspired by the original model for chiral symmetry breaking (CSB) by Nambu and Jona-Lasinio (NJL), the existence of the quark condensate has been related to the strong attractive coupling in the color singlet channel, and the quasiparticle excitations of the condensate with the same quantum numbers as the bare quarks have been studied. The massive quasiparticles are identified with the constituent quarks of the nonrelativistic quark model of hadrons. A natural question, then, is whether it is possible to influence the vacuum condensate in a way which manifests itself as a change in the hadron spectrum. One approach, which has been studied extensively, is the destruction of the condensate at high temperature, leading to a quark-gluon plasma.

Here we investigate the effect on the QCD vacuum of large external magnetic fields. An external magnetic field will localize the condensate of $Q\bar{Q}$ pairs on Landau orbits, thereby increasing the value of the condensate in the QCD groundstate. Consequently, the mass of the quasiparticle excitation—the constituent quark—increases, and hadronic excitations, as bound states of the constituent quarks, become more massive. We consider two model descriptions of chiral symmetry breaking: via a four-point quark interaction (the original NJL model) and an instanton-induced interaction term. We find that the two approaches lead to rather different results.

In the NJL model, the lagrangian for a minimally coupled external electromagnetic field to quarks with rest mass m_0 and charge q reads [1]:

$$\mathcal{L} = \bar{Q}(i\partial + qA_{\text{ext}} - m_0)Q + g [(\bar{Q}Q)^2 - (\bar{Q}\gamma_5 Q)^2]. \quad (1)$$

In order to treat chiral symmetry breaking within the mean-field approximation, we add and subtract a mass term $m_d \bar{Q}Q$ in eq. (1): $\mathcal{L} = \mathcal{L}_0 + \mathcal{L}_{\text{int}}$, with

$$\begin{aligned} \mathcal{L}_0 &= \bar{Q}(i\partial + qA_{\text{ext}} - m)Q \\ \mathcal{L}_{\text{int}} &= m_d \bar{Q}Q + g [(\bar{Q}Q)^2 - (\bar{Q}\gamma_5 Q)^2]. \end{aligned} \quad (2)$$

Here, m_o is the bare mass, m_d the dynamically generated quark mass, and $m = m_d + m_o$ the total ('constituent') mass. m_d can be determined by minimizing the vacuum action $W = - \int d^4x \mathcal{L}$ with respect to m_d .

Applying proper-time techniques, W can be computed exactly analytically for a constant external magnetic field [2]. Minimizing W with respect to m_d yields the "gap equation" for the dynamical mass m_d :

$$\frac{g}{2\pi^2} \int_{s_0}^{\infty} \frac{ds}{s^2} e^{-m^2 s} qBs \coth(qBs) = \frac{m_d}{m} . \quad (3)$$

In the limit of vanishing external field and vanishing bare mass m_o the critical value of the coupling is given by $G = 1$, where $G = \frac{g\Lambda^2}{2\pi^2}$ is the renormalized NJL coupling constant. For $m_o > 0$ one can find a solution for any value of the coupling, i.e. the critical coupling is $G = 0$.

If we fix g by demanding that for $B = 0$ the dynamically produced mass should be given by the constituent quark mass $m \sim 300$ MeV, we get an equation for the field strength dependence of the constituent quark mass $m(B)$:

$$\int_{s_0}^{\infty} \frac{ds}{s^2} \left(e^{-m(B)^2 s} qBs \coth(qBs) - \frac{m}{m_d} \frac{m_d(B)}{m(B)} e^{-m^2 s} \right) = 0 , \quad (4)$$

with $m \equiv m(B = 0)$. The resulting mass ratio $r_m(B) = m(B)/m$ determines the change of the energy scale for CSB-generated quantities such as hadron masses. In Fig. 1 we plot $r_m(B)$ for several values of the cutoff Λ with $m_o = 0$; the general behavior of the result is not greatly affected by a non-vanishing bare mass m_o .

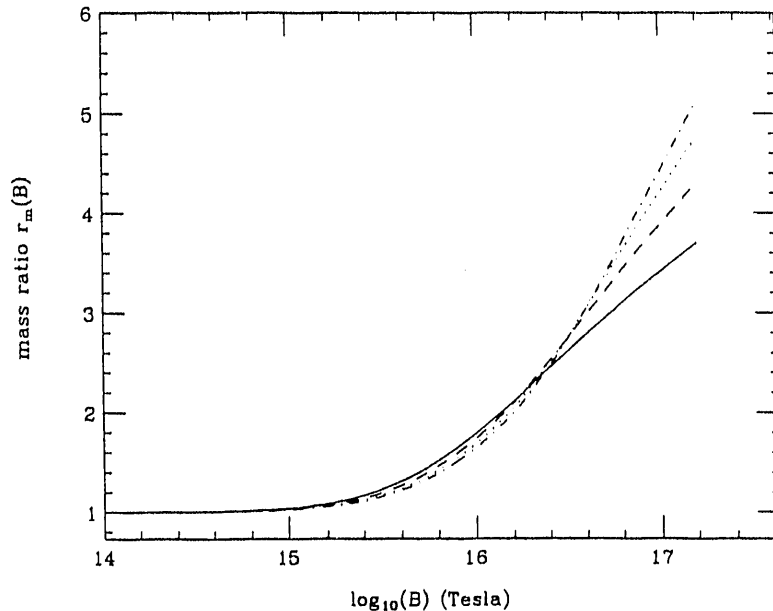


Fig. 1: Mass ratio r_m as function of the magnetic field $q^f B/e$ for an NJL interaction term. q^f is the electric charge of the quark with flavor f . The solid, dashed,

dotted, and dot-dashed lines corresponds to cutoffs $\Lambda = 0.75, 1.0, 1.25$, and 1.5 GeV, respectively.

We next study the B -dependence of the quark condensate in the case of instanton-induced chiral symmetry breaking. The interaction term is generated through the occurrence of fermionic zero-modes in the field of an instanton, effectively coupling the quark fields. Within a one-loop calculation the interaction term reads [3]:

$$\mathcal{L}_{inst} = \frac{\kappa}{8} \{ \det_f(\bar{Q}(1 - \gamma_5)Q) + \det_f(\bar{Q}(1 + \gamma_5)Q) \} \quad (5)$$

where \det_f denotes the determinant in flavor space.

Calculating the contribution to the action W one gets the result

$$W_{inst} = 8V \kappa N_c(N_c + 1)(2N_c + 1) \prod_{f=1}^3 \frac{m^f}{4\pi^2} \int_{s_0}^{\infty} \frac{ds}{s^2} e^{-(m^f)^2 s} q^f B s \coth(q^f B s). \quad (6)$$

The superscript f numbers the different flavors (u,d,s). The inclusion of the term (6) in the variation of W with respect to m_d yields the modified gap equations [4].

Since the interaction (6) couples different flavors the resulting gap equations form a system of coupled integral equations. There are six parameters: m^f ($f = 1, 2, 3$), g , κ , and Λ . The quark masses m^f are roughly given by the hadronic and mesonic spectra, while the coupling strengths and the cut-off can again be determined by the solution of for vanishing magnetic field. Taking these values one can determine the dependence of the quark masses $m^f(B)$ on the external magnetic field. In our calculations, we examined only the pure instanton interaction ($g = 0$), using the parameter values $m_u^0 = m_d^0 = 0$, $m_s^0 = 150$ MeV, $m^g = 500$ MeV.

The results for the masses are shown in Fig. 2. The flavor-coupling generates a large $SU_f(3)$ splitting. This surprising behavior is based on the bare-mass splitting of the u and d quarks as compared to the s quark. The instanton-induced coupling generates a dynamical mass of one flavor as a function of the product of the scalar condensates of the other two flavors. The strange quark contribution $\langle \bar{s}s \rangle$ is decreasing with increasing mass m_s , because the low-momentum cut-off reduces the value of the integral and compensates for the increase of the integrand with B . The u and d quark masses depend on $\langle \bar{s}s \rangle$, and so are suppressed from the outset by the larger strange quark bare mass. Physically, the $s\bar{s}$ pairs in the vacuum become more strongly localized with increasing m_s ; their interaction is then suppressed by the effects of asymptotic freedom at small distances. This suppression of the condensate is smaller for u and d quarks as compared to the gain by increasing the magnetic field. Therefore the instanton interaction generates a splitting of the mass values and the s quark mass continues to increase with larger magnetic fields. The different behavior of m_u and m_d results from the different electric charge of up and down quarks, $q_u = +2/3$, $q_d = -1/3$.

[*] S. Schramm, B. Müller, and A.J. Schramm, preprint DUKE-TH-91-13, Int. J. Mod. Phys. (in print).

[1] V. Bernard, Phys. Rev. **D34**, 1601 (1986).

- [2] S.P. Klevansky and R.H. Lemmer, Phys. Rev. **D39**, 3478 (1989).
 [3] G. 't Hooft, Phys. Rev. **D14**, 3432 (1976).
 [4] M. Takizawa, K. Tsushima, Y. Kohyama, and K. Kubodera, Nucl. Phys. **A507**, 611 (1990).

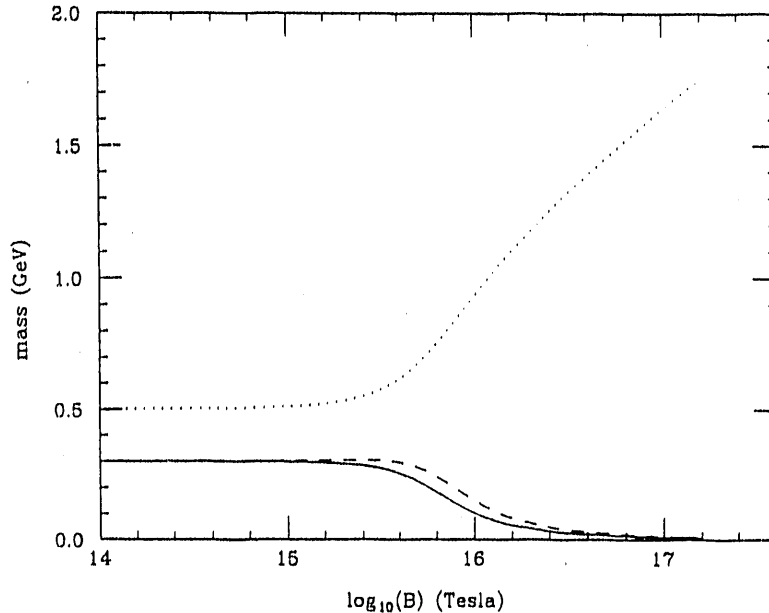


Fig. 2: Quark masses m^f as function of the magnetic field B for the instanton-induced quark interaction. The solid, dashed, and dotted lines correspond to the flavors u , d , and s , respectively.

5.4. Collective Excitations of the QED Vacuum ?

(D.C. Ionescu, W. Greiner, B. Müller, G. Soff [*])

We have investigated the possible existence of collective excitations in the electron-positron vacuum in the presence of a strong Coulomb field. The existence of modes of this type in Coulomb fields approaching critical strength ($Z \sim 170$) was suggested in earlier calculations of Lemmer and Greiner [1], based on relativistic RPA theory, and Hirata and Minakata [2], who applied a bosonization technique. If such excitation existed, they might be formed in the environment of collisions of very heavy nuclei, and their decay might explain [3] the origin of the “anomalous” e^+e^- coincidence lines observed at GSI [4].

The starting point of our investigation was the two-particle Feynman propagator

$$K(x_1, x_2, x_3, x_4) = \langle 0 | T[\psi(x_1)\psi(x_2)\psi^\dagger(x_3)\psi^\dagger(x_4)] | 0 \rangle, \quad (1)$$

where $|0\rangle$ denotes the ground state of the interacting electron-positron fields in the presence of an external Coulomb potential. Since K depends only on $\tau = t_1 - t_3$ in a static external field, it is useful to study the Fourier transformed operator $K(\omega) = \int d\tau e^{i\omega\tau} K(\tau)$, whose singularities indicate the excitation modes of the system.

The Dyson equation for K can be written in the form:

$$K(\omega) = K_0(\omega) + iK_0(\omega)W(\omega)K_0(\omega), \quad (2)$$

where the *effective interaction* W satisfies the equation:

$$W(\omega) = V + iVK_0(\omega)W(\omega), \quad (3)$$

V being the residual (Coulomb) interaction between electrons and positrons. Poles of $K(\omega)$ corresponding to collective excitations are due to poles in $W(\omega)$. We have searched for such poles within the Fock space of single particle-hole excitations, corresponding to the random phase approximation (RPA). As basis states we chose the exact single particle states in the external Coulomb field. The continuum was represented by relativistic wave packets, and the basis was restricted to $s_{1/2}$ and $p_{1/2}$ states.

The shifts in the excitation energies of single particle states due to the e^+e^- interaction was less than 0.5 percent in all our calculations. No new poles of $W(\omega)$, which would correspond to collective excitations, were found. We also evaluated relativistic transition strengths between various states, which represent a direct measure of correlation effects. The correlated transition strengths never deviated by more than 10 percent from their bare (single-particle) values. In conclusion, we found no evidence for collectivity in the electron-positron field around heavy and superheavy atomic nuclei.

- [*] D.C. Ionescu, W. Greiner, B. Müller, and G. Soff, preprint GSI-91-42.
- [1] R.H. Lemmer and W. Greiner, Phys. Lett. **162B**, 247 (1985).
- [2] Y.S. Hirata and H. Minakata, Z. Phys. C **46**, 45 (1990).
- [3] S. Midorikawa and Y. Yamaguchi, preprint INS-567, Tokyo (1986).
- [4] T. Cowan et al., Phys. Rev. Lett. **56**, 444 (1986); W. Koenig et al., Phys. Lett. **218B**, 12 (1989); P. Salabura et al., Phys. Lett. **245B**, 153 (1990).



Eric van Doorn



Chengqian Gong



Dena McCown



Berndt Müller



Jochen Rau



Alec Schramm



Atanas Trayanov



Carlos Villarreal



Xin-Nian Wang

APPENDICES

IA. Published Articles:

1. Quark-Gluon Plasma Signatures?, B. Müller, S. Schramm, *Phys. Rev. C* **43** (1991) 2791-2797.
2. Transverse Baryon Flow as Possible Evidence for a Quark-Gluon Plasma Phase, P. Levai, B. Müller, *Phys. Rev. Lett.* **67** (1991) 1519-1522.
3. Quark-Antiquark Condensates in Strong Magnetic Fields, S. Schramm B. Müller and A. J. Schramm, *Mod. Phys. Lett. A* **7** (1992) 973-981.
4. On the Suppression of the Gluon Radiation for Quark Jets Penetrating a Dense quark Gas, A. H. Sorensen, *Z. Physik C* **53** (1992) 595-600.
5. Parton Cascades in Highly Relativistic Nuclear Collisions, K. Geiger, B. Müller, *Nucl. Phys. B* **369** (1992) 600-654.
6. QCD Phenomenology of Nucleon-Nucleon Cross Sections, N. Abou-El-Naga, K. Geiger, B. Müller, *J. Phys. G* **18**.
7. Exact Dirac Propagator in a Magnetic "Sheet", S. Schramm, B. Müller, A. J. Schramm, *Phys. Lett. A* **164** (1992) 28-32.
8. W Boson Condensation in P-P Collisions?, S. Schramm, B. Müller, A. J. Schramm, *Phys. Lett. B* **277** (1992) 512-514.
9. Transverse Flow Due to Minijets in $p\bar{p}$ Collisions at $\sqrt{s} = 1.8$ TeV, X. N. Wang, M. Gyulassy, *Phys. Lett. B* (in print).
10. Gluon Shadowing and Jet Quenching in A+A Collisions at $\sqrt{s} = 200$ GeV, X. N. Wang, M. Gyulassy, *Phys. Rev. Lett.* **68** (1992) 1480-1483.
11. Dynamical versus Decay Photons in A + A Collisions at $\sqrt{s} = 200A$ GeV, D. K. Srivastava, B. Sinha, M. Gyulassy, and X. N. Wang, *Phys. Lett. B* **276** (1992) 285-289.
12. Color Screening in Relativistic Heavy Ion Collisions, T. Biro, B. Müller, X. N. Wang, *Phys. Lett. B* (in print).
13. Probing Parton Thermalization Time with Charm Production, B. Müller, X. N. Wang, *Phys. Rev. Lett.* **68** (1992) 2437-2439.
14. Medium Effects on Kaon Production, C. Gong, *Phys. Lett. G* (in print).

IB. Other Publications:

1. Vacuum Structure in Intense Fields, edited by H. M. Fried and B. Müller, NATO-ASI Series B, Vol. 255, Plenum Press (New York 1991).

IC. Submitted Articles:

1. The Origin of the Metric Structure of Space-Time, J. Rau (submitted to *J. Phys. A*)
2. Multiparticle Production in Lepton-Nucleus Collisions and Relativistic String Models, D. J. Dean, M. Gyulassy, B. Müller, E. A. Remler, M. R. Strayer, A. S. Umar, J. S. Wu (submitted to *Phys. Rev. C*)
3. Collective Excitations of the QED Vacuum?, D. C. Ionescu, W. Greiner, B. Müller, G. Soff, preprint GSI-91-42 (submitted to *Ann. Phys.*)
4. Studying Minijets via the p_T dependence of Two-Particle Correlations in ϕ , X. N. Wang (submitted to *Phys. Rev. D*)
5. Deterministic Chaos in Non-Abelian Lattice Gauge Theory, B. Müller, A. Trayanov (submitted to *Phys. Rev. Lett.*)

ID. Conference Reports:

Real-Time Evolution in Lattice Gauge Theory, A. Trayanov, B. Müller, Conference on Computational Quantum Physics, Nashville, May 1991.

Quark-Gluon Transport Theory: A Monte-Carlo Simulation, K. Geiger, B. Müller, Conference on Computational Quantum Physics, Nashville, May 1991.

Applying Neural Networks to Resonance Search in High Energy Physics, J. Rau, B. Müller, R. G. Palmer, Workshop on Neural Networks, Vietri, June 1991.

Gluon Shadowing and Jet Quenching in Relativistic Heavy Ion Collisions, X. N. Wang, M. Gyulassy, (Quark Matter '91, Nucl. Phys.)

Quark Gluon Plasma Signatures, B. Müller, (Quark Matter '91, Nucl. Phys.)

IIA. Invited Talks:

1. A. Trayanov: "Real-time Evolution in Lattice Gauge Theory", (Conf. on Computational Quantum Physics, Nashville, (May 1991).
2. B. Müller: "Quark-Gluon Transport Theory: A Monte-Carlo Simulation" (Conf. on Computational Quantum Physics, Nashville, May 1991).
3. J. Rau: "Applying Neural Networks to Resonance Search in High-Energy Physics" (Workshop on Neural Networks, Vietri, Italy, June 1991).
4. X. N. Wang: "Gluon Shadowing and Jet Quenching in Relativistic Heavy Ion Collisions" (Quark Matter '91, Gatlinburg, TN, November 1991).
5. K. Geiger: "Dynamics of Parton Cascades in Highly Relativistic Nuclear Collisions" (Quark Matter '91, Gatlinburg, TN, November 1991).

6. B. Müller: "Signatures of the Quark-Gluon Plasma" (Quark Matter '91, Gatlinburg, TN, November 1991).
7. B. Müller: "The Atomic Clock: How well does it work?" (APS Spring Meeting, Washington D.C., April 1992).

IIB. Contributed Talks and Seminars:

B. Müller: "Transversaler Baryonenfluß: Ein Hinweis auf Quark Deconfinement" (Univ. Giessen, June 1991).

B. Müller: "A Parton Cascade for Relativistic Nuclear Collisions" (Univ. Frankfurt, June 1991).

B. Müller: "A Parton Cascade for Relativistic Nuclear Collisions", (Univ. Regensburg, July 1991).

B. Müller: "Relativistic Nuclear Collisions or Probing the Very Early Universe in the Laboratory" (Univ. of Pennsylvania, October 1991).

C. Gong: "Effective Potential of a Kaon in Hot Hadronic Gas" (APS Fall Meeting, East Lansing, MI, October 1991).

B. Müller: "Parton Cascades in Highly Relativistic Nuclear Collisions" (APS Fall Meeting, East Lansing, MI, October 1991).

B. Müller: "Relativistic Nuclear Collisions: Studying the Early Universe in the Laboratory" (Univ. of Wisconsin, Madison, WI, November 1991).

B. Müller: "Preequilibrium Phenomena in Relativistic Nuclear Collisions" (Heavy Ion Forum, CERN, March 1992).

B. Müller, "Deterministic Chaos in Non-abelian Lattice Gauge Theory" (CERN, March 1992).

X.-N. Wang, "High p_T Physics in High Energy Heavy Ion Collisions", Kent State University, Kent, 13 December 1991.

X.-N. Wang, "Hard Probes of Quark Gluon Plasma", University of Washington, Seattle, 30 January 1992.

X.-N. Wang, "High p_T Processes and Quark Gluon Plasma", University of Oregon, Eugene, 5 March 1992.

X.-N. Wang, "Minijets and Thermalization in Heavy Ion Collisions", Lawrence Berkeley Laboratory, Berkeley, 11 March 1992.

X.-N. Wang, "Effects of Minijets in Heavy Ion Collisions", MIT, Boston, 16 March 1992.

X. N. Wang: "Probing Parton Thermalization with Jet Quenching and Charm Production" (APS Spring Meeting, Washington D.C., April 1992).

III. Triangle Nuclear Theory Colloquium Series

- 11/5/91 Tamas Biro (Univ. Giessen)
Confinement with Gaussian Gluon Fields
- 11/19/91 Kuniharu Kubodera (Univ. South Carolina)
Current Topics in Nuclear Weak-Interaction Processes
- 11/26/91 Nathan Isgur (C.E.B.A.F.)
A New Symmetry of the Strong Interaction
- 12/3/91 Carl M. Shakin (Brooklyn College, CUNY)
Mesonic Degrees of Freedom in Nuclei
- 12/10/91 Stanley J. Brodsky (SLAC)
Novel Phenomena in QCD
- 1/28/92 John Negele (MIT)
Hadron Structure in Lattice QCD
- 2/18/92 James Friar (Los Alamos National Laboratory)
Muon-Catalyzed p-d Fusion
- 2/25/92 Joseph Milana (College of William & Mary)
Decoupling Confinement and Chiral Symmetry Breaking
- 3/2/92 Sergei Matinyan (Erewan, Armenia):
Quark Degrees of Freedom in Nucleons and Nuclei
- 3/3/92 Joseph Kapusta (Univ. Minnesota)
Quantum Chromodynamics at High Temperature and Density
- 3/10/92 Hans Weber (Univ. Virginia)
Electromagnetic Form Factors and Structure Functions
- 3/17/92 Daniel Mustaki (Ohio State Univ.)
Compton Scattering in the Light-Cone Tamm-Dancoff Approximation
- 3/24/92 Donald Robson (Florida State Univ.)
Baryon Models
- 3/25/92 T. D. Lee (Columbia University):
The Weak Interaction, It's History and Impact on Physics
- 3/21/92 Andreas Schäfer (Univ. Frankfurt)
The Internal Spin Structure of the Nucleon and the Hermes Experiment
- 4/7/92 Shoji Nagamiya (Columbia University)
Strangeness Production in Heavy Ion Collisions at the AGS
- 4/14/92 Fred Myhrer (Univ. South Carolina)
Exclusive Hadronic Reactions and Almost Asymptotic QCD

- 4/28/92 Andreas Kronfeld (Fermilab)
 Nucleon Compton Scattering in Perturbative QCD
- 5/5/92 Carl Carlson (College of William and Mary)
 How to look for Quark Degrees of Freedom in Nuclei

IV. QCD for Nuclear Physicists

- 2/20/92 Six-hour lecture series on "QCD for Nuclear Physicists"
 -4/2/92 by Carlos Villarreal (Duke) with special emphasis on the TUNL community.

V. Theory Seminars at Duke 1991/92

- 7/7/91 Klaus Geiger (Duke Univ.):
 Quarks and Gluons in the Shower
- 8/8/91 David Dean (Vanderbilt Univ.):
 A String-Parton Model for e-A, p-p, p-A, and A-A Collisions
- 8/14/91 Nagwa Abou-El-Naga (Egyptian Univ. Kairo):
 Anomalons at Intermediate Relativistic Energy
- 8/21/91 Marjorie Klenin (North Carolina State Univ.):
 The Theory of Generalization in Backpropagation Networks
- 8/28/91 Berndt Müller (Duke Univ.):
 The Electron-Positron Puzzle
- 9/11/91 Srinivasa Rao (Institute Mathematical Sciences, Madras, India/Duke):
 Recent Developments in the Quantum Theory of Angular Momentum
- 9/18/91 Louise Dolan (Univ. North Carolina):
 Selection Rules and Vertex Constructions in String Lagrangians
- 9/25/91 Stephen Cotanch (NCSU Univ.):
 Hyperon Electromagnetic Production Studies at C.E.B.A.F.
- 10/16/91 Michael Prisant (Duke Univ. Chemistry Dept.):
 Structure, Dynamics, and Reactive Preparation of Halogen Doped
 Rare-Gas Clusters
- 10/16/91 Walter Greiner (Univ. Frankfurt):
 Nuclear Matter Under Extreme Conditions
- 10/30/91 Jun Ye (Duke Univ.):
 Diffusion in Configuration Space and Glassy Relaxation
- 11/5/91 E. D. Davis (Univ. Arizona):
 Quantum transport approach to fermion-field dynamics

- 11/6/91 Eugene F. Shender (Univ. North Carolina and Leningrad):
Order by Disorder in Quantum Antiferromagnets and Spin Nematics
- 11/8/91 Xin-nian Wang (Duke Univ.):
Particle and Mini-Jet Production in High Energy $pp, p\bar{p}$ Collisions
- 11/18/91 Hans-Thomas Elze (J.W. Goethe-Univ. Frankfurt):
Ginsburg-Landau Theory for Multiparticle Correlations
- 11/20/91 Henri Ruegg (Univ. Geneva):
Introduction to Quantum Groups
- 11/20/91 Ulrich Heinz (Univ. Regensburg, Germany):
Vector mesons as probes of the Hadronic fireball
- 12/4/91 Xin-nian Wang (Duke Univ.):
Energy Loss of a Fast Parton in Dense Matter
- 12/11/91 Stanley J. Brodsky (SLAC):
QCD on the "Light Cone"
- 12/16/91 K. Srinivasa Rao (Inst. Mathematical Sciences, Madras, India):
The Life and Work of Ramanujan
- 1/22/92 Carlos Villarreal (Duke Univ. and UNAM, Mexico City):
Quantum Fluctuations in Waveguides and Cavities
- 1/29/92 Max A. Lohe (Univ. Northern Territory/Duke):
Solitons in Chern-Simons Gauge Theories
- 2/5/92 Jerry Bernholc (North Carolina State Univ.):
Quantum Molecular Dynamics Studies of Materials
- 2/12/92 James W. York (Univ. North Carolina):
Time and Temperature in the Geometry of a Rotating Black Hole
- 2/12/92 Nathan Isgur (CEBAF):
Mysteries of the Strong Interaction
- 2/13/92 Michael Musolf (MIT):
Parity Violating Electron Scattering
- 2/18/92 Roxanne Springer (Univ. Wisconsin-Madison):
What Can B-Mesons Tell us about the Standard Model?
- 2/18/92 Roxanne Springer (Univ. Wisconsin-Madison):
An Effect of Strangeness in the Nucleon on Parity Violation
- 2/19/92 Henry Greenside (Duke/ Computer Science):
The Equilibrium Problem of Magnetically Confined Fusion Plasmas
- 2/20/92 Suzhou Huang (Univ. of Washington):
The Relevance of Dilute Instantons Ensemble to Light Hadrons

- 2/25/92 Stefan Schramm (Caltech):
The QCD Vacuum Hadron Structure, and the Influence of Large
Electromagnetic Fields
- 2/26/92 Stefan Schramm (Caltech):
Pycnonuclear Reactions in Stellar Matter
- 2/28/92 Sergei Matinyan (Erewan, Armenia):
Chaotic Dynamics in Non-Abelian Gauge Theories
- 3/4/92 Joe Kapusta (Univ. Minnesota):
Dynamics of Relativistic First Order Phase Transitions
- 3/11/92 P. Levai (Budapest/Duke):
Mesons in Dense Hadronic Matter
- 3/25/92 T. D. Lee (Columbia University):
Buckyballs and Superconductivity
- 3/30/92 Klaus Geiger (Univ. of Minnesota)
Thermalization in High-Energy Nuclear Collisions
- 4/1/92 Richard Palmer (Duke Univ.):
Recent Developments in Artificial Life and Adaptive Computation
- 4/1/92 Steven E. Koonin (Caltech):
Global Change and the Dark of the Moon

**DATE
FILMED**

7 / 14 / 92

